nature physics

REVIEW ARTICLE

PUBLISHED ONLINE: 29 AUGUST 2010 | DOI: 10.1038/NPHYS1759

High-temperature superconductivity in iron-based materials

Johnpierre Paglione* and Richard L. Greene

The surprising discovery of superconductivity in layered iron-based materials, with transition temperatures climbing as high as 55 K, has led to thousands of publications on this subject over the past two years. Although there is general consensus on the unconventional nature of the Cooper pairing state of these systems, several central questions remain — including the role of magnetism, the nature of chemical and structural tuning, and the resultant pairing symmetry — and the search for universal properties and principles continues. Here we review the progress of research on iron-based superconducting materials, highlighting the main experimental benchmarks that have been reached so far and the important questions that remain to be conclusively answered.

In February 2008, Hideo Hosono and co-workers reported the discovery of 26 K superconductivity in fluorine-doped LaFeAsO (ref. 1), marking the beginning of worldwide efforts to investigate this new family of superconductors. Although rumours of a 50+ K superconductor swirled around the 2008 APS March meeting in New Orleans, researchers in Japan and China were busy with experiments that would largely advance this field to its present status by raising superconducting transition temperature (T_c) values of LaFeAs(O, F) to 43 K by application of pressure[2], and then as high as 55 K by replacement of La by other rare-earth elements (see ref. 3 for details). Historically, the typically antagonistic relationship between superconductivity and magnetism has led researchers to avoid using magnetic elements — ferromagnetic in particular — as potential building blocks of new superconducting materials. Because elemental iron is strongly magnetic, the discovery of Fe-based superconductors (FeSCs) with high T_c values was completely unexpected. This has opened a new avenue of research driven by the fact that our fundamental understanding of the origins of superconductivity needs significant improvement.

This Review Article provides a summary update on some of the recent experimental results and an overview of the status of the field. Our goal is to highlight important experimental observations and theoretical perspectives that may lead to a consensus on the understanding of superconductivity in the FeSCs. Some results have been omitted owing to space and citation limitations, so we encourage the reader to consult more detailed overviews in existing reports[3,4]. The basic behaviour of several classes of FeSCs is now known to be similar, so this Review will cover universal properties but will also focus on the class of intermetallic FeSCs with the $ThCr_2Si_2$ (122) structure, pointing out any significant differences from the other systems.

Crystal structures and tuning parameters

So far, five different structural classes of FeSCs have been found. These structures, shown in Box 1, all share a common layered structure based on a planar layer of iron atoms joined by tetrahedrally coordinated pnictogen (P, As) or chalcogen (S, Se, Te) anions arranged in a stacked sequence separated by alkali, alkaline-earth or rare-earth and oxygen/fluorine 'blocking layers'. It is now widely thought that the interaction that leads to the high-T_c superconductivity originates within these common iron layers, similar in nature to the common copper–oxygen building block found in the copper oxide (cuprate) high-T_c superconductors. As in the cuprates, chemical substitution also plays a key role in inducing the superconducting phase in iron pnictides. However three key differences are found: (1) in the arrangement of pnictogen/chalcogen anions above and below the planar iron layer (see Box 1) as opposed to the planar copper–oxygen structure of the cuprates; (2) in the ability to substitute or dope directly into the active pairing layer; and (3) in the metallic (rather than insulating) multiband nature of the parent compounds. It is these traits, together with the similar interplay of magnetism and superconductivity, that mark the iron pnictides and cuprates as distinct, but closely related, superconducting families. The phase diagram of the FeSCs is in fact strikingly similar to those of several other classes of unconventional superconductors, including the cuprates, organics and heavy-fermion superconductors, all believed to harbour unconventional (non-phonon-mediated) pairing mechanisms. Although the mediator of pairing in these systems remains officially unidentified, a large amount of circumstantial evidence points to magnetic spin fluctuations: in all cases magnetism must be suppressed, either by pressure or doping, before optimal bulk-phase superconductivity appears. Although their more metallic nature may place them closer to the heavy-fermion systems (metallic magnetism) than to cuprates (Mott-insulator physics), the striking resemblance of interpenetrating ground states in these systems deserves strong attention in devising a generalized theory of unconventional superconductivity.

The generic phase diagram of the FeSC systems can be produced by manipulating the chemical or structural properties, using either chemical doping/substitution or applied external pressure to drive an antiferromagnetic (AFM), non-superconducting parent compound to a superconducting (SC), non-AFM state. A compilation of experimental phase diagrams is presented in Fig. 1 for the Ba-based 122 system, so far the most studied of the five families and widely thought to capture the main traits of all FeSCs. In $BaFe_2As_2$, the systematic substitution of either the alkaline-earth (Ba), transition-metal (Fe) or pnictogen (As) atom with a different element almost universally produces the phase diagram presented

Center for Nanophysics and Advanced Materials, Department of Physics, University of Maryland, College Park, Maryland 20742, USA.
*e-mail: paglione@umd.edu.

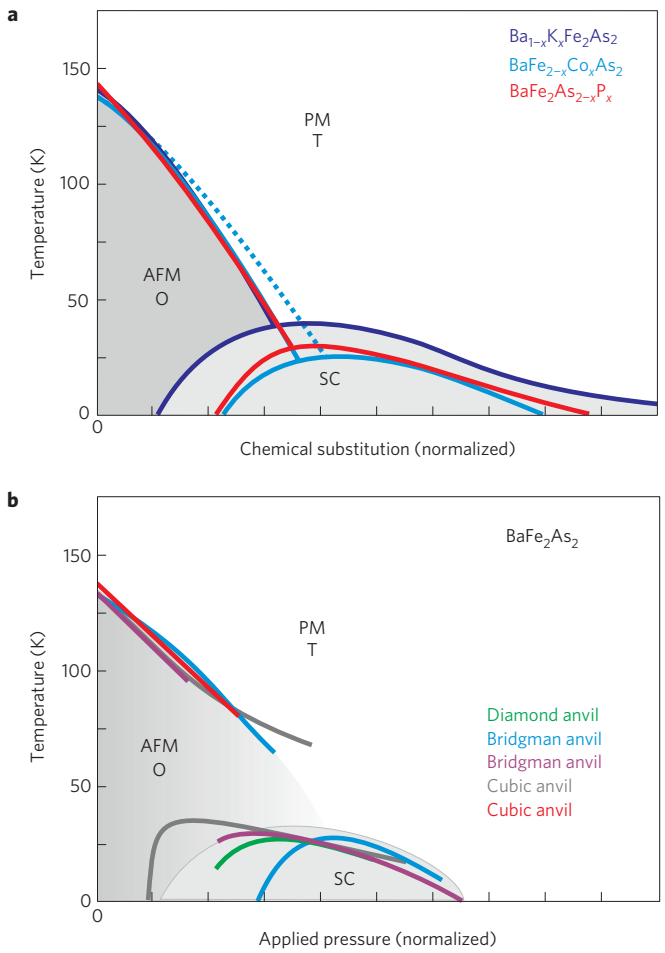

Figure 1 | Experimental phase diagrams of the $BaFe_2As_2$ system. **a**, Chemical-substitution phase diagram of the $BaFe_2As_2$ system, shown for K (ref. 7), Co (ref. 8) and P (ref. 9) substitutions, with the amount of chemical substitution (x) normalized to overlap the descent of the AFM transition for simplified comparison of the relative position of the SC phase. The dotted line indicates the structural transition between tetragonal (T) and orthorhombic (O) crystallographic phases observed for Co substitution, which is coincident with the paramagnetic (PM) to AFM transition in the parent compound $BaFe_2As_2$ (ref. 8). **b**, Applied-pressure phase diagram for $BaFe_2As_2$ as a function of external pressure applied under various levels of hydrostaticity, using diamond anvil cell[17], Bridgman[18,19] and cubic anvil cell[20,21] techniques. Note that the pressure axis is normalized to overlap the descent of the antiferromagnetic transitions for each experiment for simplified comparison.

in Fig. 1a, composed of coupled AFM and structural transitions that are suppressed with substitution and an SC phase that is more or less centred near the critical concentration where AFM order is destroyed. This is somewhat different from the known behaviour of fluorine-doped '1111' systems such as $LaFeAsO_{1-x}F_x$ (ref. 5), where AFM and SC phases are completely separated as a function of doping and do not overlap. However, the coexistence of AFM and SC phases such as reported for $SmFeAsO_{1-x}F_x$ (ref. 6) is believed to probably be the more intrinsic property of the generic FeSC phase diagram, motivating efforts to study the 122-type systems in great detail. The quantitative similarity between phase diagrams produced by substitutions involving both obvious (that is, K^{1+} for Ba^{2+}; ref. 7) and subtle (that is, Co-$3d^7$ for Fe-$3d^6$; ref. 8) charge doping, as well as nominally isovalent (P-$3p^3$ for As-$4p^3$; ref. 9) substitutions, is enticing owing to the implied versatility of chemical tuning parameters available to experimentalists for studying these systems. Furthermore, it promotes the idea that simple charge doping is not the sole factor in determining the phase boundaries of these systems and that structural tuning may play a role.

However, subtleties in the electronic structure of these materials, as discussed below, make the situation more complex than that of a simple structural tuning effect. This is highlighted by the sensitivity of the superconducting phase to the particular choice of ion substituent. For example, superconductivity in the 122-type materials, first shown to occur by Co substitution for Fe in $SrFe_2As_2$ (ref. 10) and $BaFe_2As_2$ (ref. 11), can be stabilized by several types of d-metal substitution. This includes the use of any elements in the Fe, Co and Ni columns (except, so far, Os; ref. 12), but excludes Cr (ref. 13), Mn (ref. 14) and Cu (ref. 15), which all act to suppress magnetism without stabilizing a high-T_c SC phase. It is thought that these latter anomalous cases arise for varying reasons to do with the unfavourable manipulation of Fe bonding and magnetism, giving clues regarding the correct distinction between charge doping and chemical substitution.

Pressure tuning is less well understood. In some cases this powerful control parameter is aligned with its chemical-substitution counterpart. For instance, in $Ba_{1-x}K_xFe_2As_2$ a good overlap exists between lattice-parameter variation by applied pressure or K substitution[16], enabling conclusions about the roles of lattice structure versus charge doping to be made. In contrast, in pressure experiments on $BaFe_2As_2$, differing experimental conditions impose variations from true hydrostatic conditions, making it difficult to generically compare phase diagrams obtained through applied pressure versus chemical substitution. Figure 1b presents a comparison of five studies[17–21] on our model 122 system using differing techniques, showing that AFM order is suppressed in a manner similar to chemical substitution in all cases shown but with differing rates. Moreover, the pressure range where the superconducting dome is located also varies for each experiment. This is probably due to the fact that the compressibility of the 122-type materials is highly anisotropic, imposing a sensitivity to non-hydrostatic pressure conditions that may alter the evolution of the phase diagram under differing experimental conditions. Such a scenario was recently shown conclusively in a comparison of pressure experiments using the same crystals but different levels of hydrostaticity[22]. Moreover, a structural phase transition (T_0) — from tetragonal at high temperatures to orthorhombic at low temperatures — is consistently found to be coupled to the AFM transition at T_N, and is either pinned directly to T_N or is separated in temperature on chemical substitution, as shown by the dashed line in Fig. 1a. Although this feature may be a key element in understanding, for instance, the nature of magnetic order as discussed below, it also poses problems in controlling hydrostaticity in a pressure experiment.

In one extreme case involving pressure-tuning of $CaFe_2As_2$, an instability to another structural phase transition (to the so-called collapsed-tetragonal phase) imposes a more severe sensitivity to anisotropic strain conditions, with a pressure-induced SC phase only present when non-hydrostatic conditions are imposed[23]. Although it remains unclear what role structure plays in stabilizing superconductivity in $CaFe_2As_2$, some theoretical ideas[24] suggest interlayer As–As bonding to be the key ingredient. The sensitivity to hydrostaticity certainly implies that a strain mechanism is at work, possibly similar to what causes the intermittent appearance of 20 K superconductivity in undoped, unpressurized 122-type parent compounds[25]. Indeed, strain effects have been identified in studies of twin domain boundaries of $BaFe_{2-x}Co_xAs_2$ using scanning superconducting quantum interference device (SQUID) microscopy, where an enhanced susceptibility at twin boundaries has been associated with an enhanced superfluid density[26]. More generally, one of the distinguishing features of the FeSC materials is the fact that the generic phase diagram can be experimentally tuned by any of several different means that allow for a precise control

Box 1 | The iron-based superconductor family.

Iron, one of the most common metals on earth, has been known as a useful element since the aptly named Iron Age. However, it was not until recently that, when combined with elements from the group 15 and 16 columns of the periodic table (named, respectively, the pnictogens, after the Greek verb for choking, and chalcogens, meaning 'ore formers'), iron-based metals were shown to readily harbour a new form of high-temperature superconductivity. This general family of materials has quickly grown to be large in size, with well over 50 different compounds identified that show a superconducting transition that occurs at temperatures approaching 60 K, and includes a plethora of different variations of iron- and nickel-based systems. So far, five unique crystallographic structures have been shown to support superconductivity. As shown in Fig. B1a, these structures all possess tetragonal symmetry at room temperature and range from the simplest α-PbO-type binary element structure to more complicated quinternary structures composed of elements that span the entire periodic table.

The key ingredient is a quasi-two-dimensional layer consisting of a square lattice of iron atoms with tetrahedrally coordinated bonds to either phosphorus, arsenic, selenium or tellurium anions that are staggered above and below the iron lattice to form a chequerboard pattern that doubles the unit-cell size, as shown in Fig. B1b. These slabs are either simply stacked together, as in FeSe, or are separated by spacer layers using alkali (for example, Li), alkaline-earth (for example, Ba), rare-earth oxide/fluoride (for example, LaO or SrF) or more complicated perovskite-type combinations (for example, $Sr_3Sc_2O_5$). These so-called blocking layers provide a quasi-two-dimensional character to the crystal because they form atomic bonds of more ionic character with the FeAs layer, whereas the FeAs-type layer itself is held together by a combination of covalent (that is, Fe–As) and metallic (that is, Fe–Fe) bonding.

In the iron-based materials, the common FeAs building block is considered a critical component to stabilizing superconductivity. Because of the combination of strong bonding between Fe–Fe and Fe–As sites (and even interlayer As–As in the 122-type systems), the geometry of the $FeAs_4$ tetrahedra plays a crucial role in determining the electronic and magnetic properties of these systems. For instance, the two As–Fe–As tetrahedral bond angles seem to play a crucial role in optimizing the superconducting transition temperature (see the main text), with the highest T_c values found only when this geometry is closest to the ideal value of ~109.47°.

Long-range magnetic order also shares a similar pattern in all of the FeAs-based superconducting systems. As shown in the projection of the square lattice in Fig. B1b, the iron sublattice undergoes magnetic ordering with an arrangement consisting of spins ferromagnetically arranged along one chain of nearest neighbours within the iron lattice plane, and antiferromagnetically arranged along the other direction. This is shown on a tetragonal lattice in the figure, but actually only occurs after these systems undergo an orthorhombic distortion as explained in the main text. In the orthorhombic state, the distance between iron atoms with ferromagnetically aligned nearest-neighbour spins (highlighted in Fig. B1b) shortens by approximately 1% as compared with the perpendicular direction.

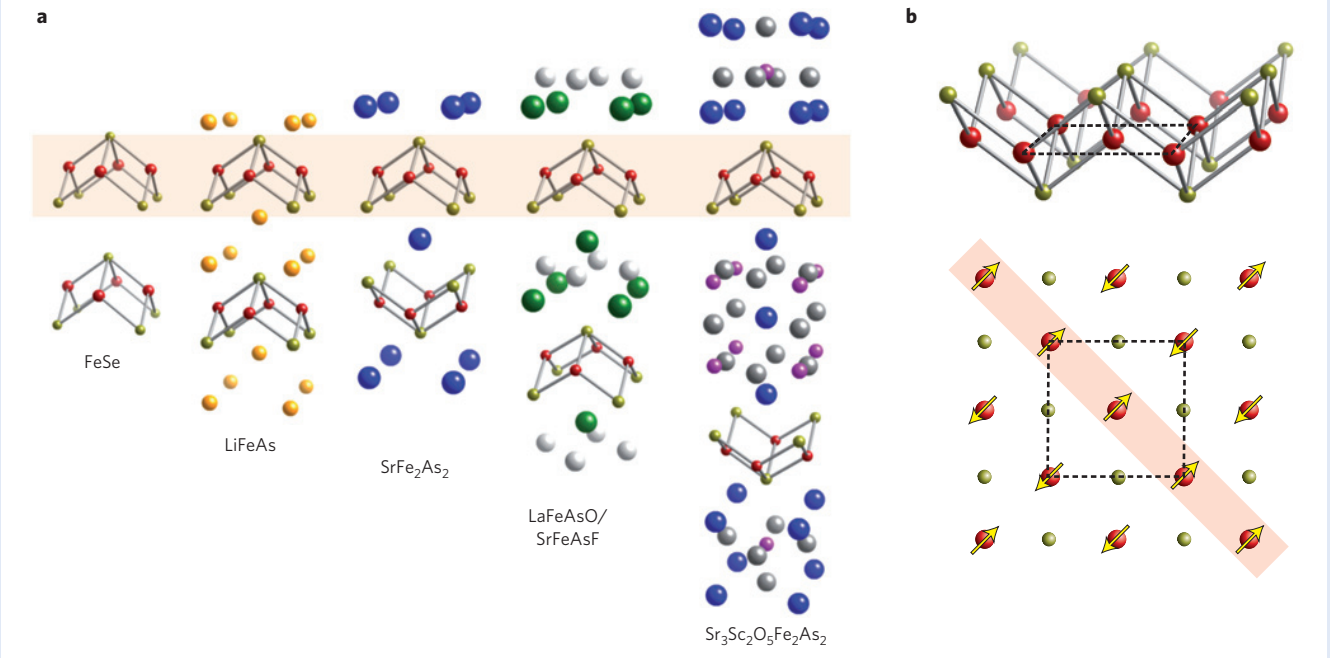

Figure B1 | Crystallographic and magnetic structures of the iron-based superconductors. a, The five tetragonal structures known to support superconductivity. **b**, The active planar iron layer common to all superconducting compounds, with iron ions shown in red and pnictogen/chalcogen anions shown in gold. The dashed line indicates the size of the unit cell of the FeAs-type slab, which includes two iron atoms owing to the staggered anion positions, and the ordered spin arrangement for FeAs-based materials is indicated by arrows (that is, not shown for FeTe).

of structural parameters, disorder location, chemical bonding and density. This is one of the key properties that has led to a rapid but in-depth understanding of these materials. In due time, controlled experimental comparisons — for instance of Hall effect (carrier density) under pressure versus doping, of different chemical substitution series and further understanding of the local nature of chemical substitution — will help pinpoint the important tuning parameters for these systems.

Electronic structure

With an interplay of magnetic and electronic interactions probably playing an integral role in determining the shape of the phase diagram of all FeSC systems, much work has gone into determining the magnetic and electronic structures of these materials. In general, these materials are well described as consisting of two-dimensional (2D) metallic sheets derived from Fe *d* states hybridized with As *p*-orbital-derived bands, sitting in a quasi-ionic framework composed of rare-earth, oxygen, alkali or alkaline-earth blocking layers (see Box 1). This arrangement unites to produce a metallic material with nominal Fe valence of 2+, low carrier concentration and high electronic density of states dominated by Fe *d* states[27]. On the basis of this FeAs-layered framework, the electronic band structure has been calculated using the local density approximation (see ref. 27 for an overview), showing that the electronic properties are dominated by five Fe *d* states at the Fermi energy, with a Fermi surface (FS) consisting of at least four quasi-2D electron and hole cylinders (see Box 2). These consist of two hole pockets centred at the Brillouin zone (BZ) centre and two electron pockets centred at $(0,\pm\pi)$ and $(\pm\pi,0)$ in the tetragonal unit cell. Two non-equivalent As positions (staggered above and below the Fe lattice) result in the folding of the BZ to include two Fe atoms per unit cell and to put the electron pockets at $(\pm\pi,\pm\pi)$ as shown in Fig. B2b, the same direction of AFM ordering vector as discussed below. A fifth hole band is also proposed to sit at $(0,\pm\pi)$ in the folded BZ, and its presence may be very sensitive to structural details[28].

The qualitative agreement with experiment is remarkably good, as shown by several angle-resolved photoemission spectroscopy (ARPES) and quantum oscillation measurements. Initial ARPES studies on LaFePO (ref. 29), $NdFeAsO_{0.9}F_{0.1}$(ref. 30) and $Ba_{0.6}K_{0.4}Fe_2As_2$ (ref. 31) all confirmed the predicted band structure consisting of hole pockets at the BZ centre and electron pockets at the BZ corners. Quantum oscillation experiments carried out on paramagnetic P-doped $BaFe_2As_2$ (ref. 32) also reveal an unreconstructed FS consistent with this basic structure, and measurements on the $BaFe_2As_2$, $SrFe_2As_2$ and $CaFe_2As_2$ parent compounds are also consistent if we take into account the BZ reconstruction due to AFM ordering[33]. As is usual, the details reveal more: simple 2D models may not capture subtle but important details of the true band structure, and three-dimensional (3D) aspects may have important implications for magnetism and superconductivity. Although ARPES is a surface probe, it is capable of probing $\mathbf{k_z}$ dispersion to a limited extent, and several studies[4] have reported strong modulation along the $\mathbf{k_z}$ direction at the BZ centre in agreement with theory[34]. Also, Compton scattering measurements, which are a bulk probe of the occupied states, are consistent with strong three-dimensionality in optimally doped $BaFe_{2-x}Co_xAs_2$ (ref. 35).

Despite being another area of active debate, the effect of hole/electron doping on the electronic structure is fairly well captured by a rigid-band picture: the basic FS topology is kept with both electron (that is, in $BaFe_{2-x}Co_xAs_2$(ref. 36)) and hole (that is, in $Ba_{1-x}K_xFe_2As_2$ (ref. 37)) doping, with the size of FS pockets changing accordingly and with reasonable continuity observed when crossing between each case[38]. Once again, however, it seems that charge doping is not the only mechanism by which this tuning can be achieved. For instance, isovalent substitutions would not be expected to mimic charge-doping effects; however, the nominally isovalent substitutions of P for As (ref. 39) and Ru for Fe (ref. 40) in $BaFe_2As_2$ indeed cause substantial changes to the Hall coefficient, even changing sign in the latter case. Moreover, a comparable scaling of FS pocket size has been shown to occur as a function of isovalent As/P substitution[32], and density functional theory (DFT) calculations suggest that the main effect of charge doping is not on the density of states, but rather on the disruption of nesting and the relative size of electron and hole pockets[34]. Beyond isovalent substitution, a recent DFT study of the local nature of *d*-electron 'dopant' ions (including the likes of Co and Ni) concluded that the extra electrons actually remain predominantly localized at the substituent site, and may act mainly to disrupt nesting properties rather than changing charge density[41]. This remains to be verified experimentally.

More profound changes in band structure may also be at play. ARPES studies of $BaFe_{2-x}Co_xAs_2$ provide indications of a possible Lifshitz transition where hole pockets disappear, enabling superconductivity to thrive[42]. A change in effective dimensionality across the AFM transition — with the development of a 3D ellipsoid in $CaFe_2As_2$ below T_0 — has been suggested to be important for superconductivity[43], but is in conflict with the observation of significant 3D structure in $BaFe_{2-x}Co_xAs_2$ outside the AFM phase[44]. Furthermore, a qualitative change in band structure seems to occur as a function of Co doping at the onset of the SC phase, as observed in ARPES (ref. 42) and Hall data[45], and is also supported by transport data[46].

The connection between structural details of FeSC materials and their seemingly sensitive electronics is an important aspect of superconductivity in the FeSCs. An empirical relationship between the tetrahedral bond angle of the As–Fe–As layer and T_c values for different FeSCs was recognized early on, with optimal T_c values suggested to be promoted by ideal tetrahedral geometry[47]. This has important implications, both theoretically and in practical terms: a close relationship between structure and superconductivity, direct or indirect, places constraints on both the theoretical understanding of the pairing interaction and the promise of superconductors with higher T_c values. Although it seems that this relationship is not universal (a notable exception includes $CsFe_2As_2$, with $T_c = 2.6$ K and As–Fe–As bond angle very close to the ideal value of 109.47°; ref. 48), it remains true that the highest-T_c FeSCs are still clustered close to the ideal tetrahedron geometry. A proposed sensitivity of electronic structure and/or magnetic interactions to details of the internal structure of the Fe–As layers is probably relevant to unravelling this puzzle. For example, calculations of the dependence of nesting in the band structure, and consequently pairing in a spin-fluctuation-mediated scenario, show a sensitivity of an extra (third) hole pocket to pnictogen height above the Fe plane with consequences for pairing symmetry[28].

Magnetism

The nature of magnetism in the FeSC parent compounds is a hotly debated topic, largely owing to its implications for the pairing mechanism: the electronic structure suggests that the same magnetic interactions that drive the AFM ordering also produce the pairing interaction for superconductivity[49]. As predicted before experiments[50], AFM order in all FeAs-based superconducting systems is found to have a wave vector directed along (π,π) in the tetragonal unit cell with a real-space spin arrangement consisting of AFM stripes along one direction of the Fe sublattice and ferromagnetic stripes along the other (see Box 1), with an ordered moment typically smaller than one Bohr magneton[51,52]. This is much smaller than that of metallic Fe, presenting a challenge for first-principles calculations, which predict a much larger moment when using the real unit-cell parameters[27]. Early on, theoretical calculations found these materials to lie near a Stoner instability, suggesting inherent itinerant magnetism[27], which could potentially explain the consistent overestimates of the ordered moment size. However, this ordering arrangement also falls naturally out of a local-moment 'J_1–J_2' model with nearest-(J_1) and next-nearest-(J_2) neighbour exchange interactions such that $J_1 < 2J_2$ (ref. 53), and hence a lot of effort has gone into determining whether such a localized model holds any validity for a system that is clearly metallic.

Box 2 | Electronic band structure and pairing symmetry.

The manner in which electrons in a solid behave, in the presence of one another and the surrounding ionic lattice, is well captured by one of the staples of condensed-matter physics known as band theory. A metal's band structure can convey a simple yet quantitative description of its electronic, optical and structural properties, and is the basis for understanding many exotic phenomena. In metals, the energy states that participate in determining most properties of a material lie in close proximity to the Fermi energy, E_F, the level below which available energy states are filled (and therefore unavailable) owing to Pauli exclusion.

The band structures of the iron-based superconducting materials have been calculated using first-principles DFT, finding good general agreement with experimental measurements (see main text). The dominant contribution to the electronic density of states at E_F derives from metallic bonding of the iron *d*-electron orbitals in the iron–pnictogen (or chalcogen) layer. These form several bands that cross E_F, both electron- and hole-like, resulting in a multiband system dominated by iron *d* character. As shown in Fig. B2a for the case of Co-doped $BaFe_2As_2$, the electronic structure is visualized as several distinct sheets of FSs within the BZ, each corresponding to a different band that crosses E_F.

Instabilities of this electronic structure to both magnetic ordering and superconducting pairing are widely believed to be at the heart of the exotic properties of the iron-based superconducting materials. For instance, in Fig. B2a we can see that a magnetic ordering vector that spans from the centre of the BZ at $\mathbf{k} = (0,0)$ ($\mathbf{\Gamma}$ point) to the corner at $\mathbf{k} = (\pi,\pi)$ ($\mathbf{M}$ point) will easily nest a circle of points on each of two different FS sheets (for example, purple and red sheets), resulting in a spin-density wave order that is driven by properties of the band structure.

Superconductivity is another very well known phenomenon that also results in an 'ordered' state that has a strong tie to the band structure. The superconducting order parameter (OP) $\mathbf{\Delta}$, or 'gap function', is a complex function with both amplitude and phase that describes the macroscopic quantum state of Cooper pairs. Its amplitude can in general depend on momentum direction and can change sign through its phase component, but in the simplest case is isotropic (*s*-wave symmetry) and therefore has a constant value for all momenta. Details of the pairing potential can instil a less simple case that involves a variation of amplitude as a function of $\mathbf{k}$, or even a variation in phase that results in a change in the sign of $\mathbf{\Delta}$ that necessitates the presence of zeroes or 'nodes' that can take on lower symmetries (*d* wave, *f* wave, and so on).

Figure B2b presents three possible scenarios for the superconducting OP symmetry in the iron-based superconductors. With the simplest *s*-wave gap symmetry (that is, with constant phase), widely ruled out by experimental evidence (see main text), more complicated scenarios are required to explain all observed properties. In particular, circumstantial evidence supports a picture where a change in the sign of $\mathbf{\Delta}$ must occur somewhere in the BZ. With multiple FSs, which is the case for FeAs-based materials, this can be realized by positioning a node either away from the Fermi energy (so-called $s\pm$) or directly at the Fermi energy (*d* wave or lower symmetry). Moreover, a modulation of the gap amplitude can occur such that, even in the *s*-wave case, so-called accidental nodes are present on at least some FSs, enabling low-energy excitations to flourish even at temperatures much below the energy of the gap.

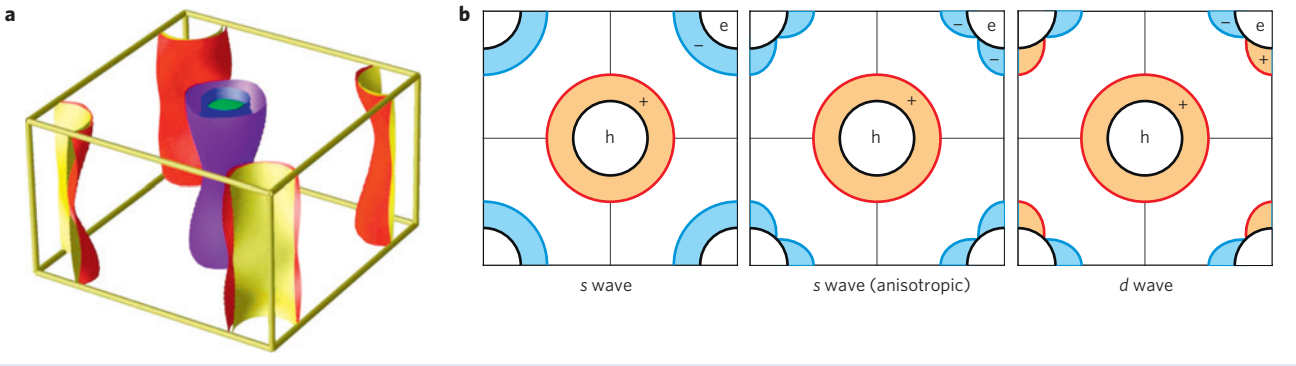

Figure B2 | Fermiology and superconducting OP symmetry of 122-type iron-based superconductors. a, FSs of $BaFe_2As_2$ with 10% substitution of Co, calculated using DFT using experimental atomic positions and drawn using the folded BZ representation with two Fe per unit cell (from ref. 49). The hole-like FS pockets (purple and blue) are centred on the $\mathbf{\Gamma}$ point [$\mathbf{k} = (0,0)$] and the electron-like surfaces are at the $\mathbf{M}$ point ([$\mathbf{k} = (\pi,\pi)$]). **b**, Schematic of the two-dimensional ($\mathbf{k}_x$–$\mathbf{k}_y$) projection of the BZ of superconducting FeAs-based materials, with multiple bands reduced to single hole (h) and electron (e) pockets. The proposed multiband pairing gap symmetries, drawn as shaded regions on hole (red) and electron (blue) pockets, are shown for an $s\pm$ structure with isotropic gaps (left) and anisotropic gaps with accidental nodes on the electron pocket (middle), and for a *d*-wave symmetry (right).

From the itinerant side, most models focus on a spin-density wave (SDW) instability of the FS. Although there are not many direct observations of an SDW energy gap, optical studies of $BaFe_2As_2$ and $SrFe_2As_2$ have indeed shown evidence for gapping of the FS below T_N (ref. 54). It is widely thought that the SDW instability arises from the nesting of two FS pockets by a large $\mathbf{Q} = (\pi,\pi)$ vector that is commensurate with the structure. This vector corresponds to the magnetic ordering vector measured throughout the FeAs-based parent compounds as well as that for magnetic fluctuations in the superconducting compounds[51,52]. There is varied, but good, evidence for (π,π) FS nesting across the entire FeSC family, as indicated by ARPES measurements of $BaFe_{2-x}Co_xAs_2$ (refs 38,55) and $Ba_{1-x}K_xFe_2As_2$ (refs 31,37) and quantum oscillation measurements in LaFePO (ref. 56) and overdoped $BaFe_2As_{2-x}P_x$ (ref. 57). In addition, the closely related material FeTe also exhibits nesting in the same (π,π) direction, even though its magnetic ordering vector is shifted by 45° at $(\pi,0)$ (ref. 58).

In the parent compounds, there are differing results regarding the change in band structure through the magnetic transition as

interpreted using ARPES data, but bulk measurements of electronic structure are more consistent. All studies[33] observe small FS pockets consistent with band-structure calculations that consider a conventional band-folding picture of the AFM ground state involving quasiparticles in a conventional SDW model. Although the general picture is well fitted with an SDW model, there are problems with matching to a purely itinerant scenario. In particular, there is significant, non-trivial reconstruction of the FS below T_N that goes beyond simple band-folding (for example, see ARPES data on $SrFe_2As_2$ and $BaFe_2As_2$ (ref. 59). Theoretically, these concerns can be taken into account in an itinerant scenario by considering details of the multiband structure[60,61], with the non-trivial band folding and metallic nature of the FeSCs probably a result of partial gapping of the FS.

From the local side, magnetic frustration is another way to explain the anomalously low moment size. Although these materials are indeed metals, local-moment models at the very least find use in describing experimental results. Neutron-scattering measurements of $CaFe_2As_2$ have revealed magnetic spin-wave excitations to live up to ~200 meV, with low-energy modes that can be phenomenologically fitted to a local-moment 3D Heisenberg model[62,63]. One study[62] observes strong damping at high energies consistent with the presence of particle–hole excitations, whereas another[63] does not observe this damping but argues that a large in-plane anisotropy of local-moment interactions, together with the incompatibility of a spin-1/2 model with even-numbered electrons in Fe-3d^6, necessitates the presence of an itinerant component. Above all, it is safe to say that these materials are 'itinerant by definition'[51], because calculations suggest that all Fe-based bands cross the Fermi energy and thus intimately involve conduction electrons in forming the magnetic state. However, we should not exclude the applicability of other alternative scenarios (see ref. 52 for details), including orbital order[64], coexistent[65] itinerant electrons and local moments, or an admixture of both local coupling and itinerant one-electron interactions[66]. In the latter case, the possibility that a nesting feature merely directs the ordering wave vector of local moments formed independent of the FS morphology is a tantalizing prospect that explains many of the observed properties.

Regardless of the exact nature of magnetic order, it is clear that magnetostructural coupling is prevalent throughout the FeSC family in the form of coupled magnetic and structural transitions. This is generally understood to be driven by magnetic interactions[27,53]. However, a peculiarity of the coupled transitions is that, aside from the case of the 122-type parent compounds where T_N and T_0 coincide exactly, the structural and magnetic phase transitions are positioned at different temperatures in 1111-type compounds, with the structural transition actually preceding the magnetic transition[67]. A comparison of this phenomenon in samples of CeFeAsO with differing levels of disorder (polycrystal, cluster, single crystal) has shown the splitting to decrease (from 18 to 6 K) with improved sample quality[68]. Considering that the splitting between T_N and T_0 is established in 122-type compounds only after chemical substitution[8,69], it is tempting to conclude that disorder is the cause of the splitting. However, an intrinsic mechanism for this splitting cannot be ruled out, especially considering the early prediction of an Ising phase transition that should precede T_N (ref. 70). Furthermore, an investigation of $Ba_{0.84}K_{0.16}Fe_2As_2$ samples with both magnetic/structural and superconducting transitions has shown that the magnetic and structural transitions are indeed separated in crystals with excellent homogeneity[71], as opposed to previous reports. It will thus be interesting to see whether experiments that tune effective dimensionality and/or magnetic coupling will reveal further insight into the nature of this splitting.

Finally, a direct coupling between structural distortion and magnetism has also been shown in P-doped CeFeAsO, where neutron scattering measurements reveal an ordered AFM moment of Fe to be linearly proportional to orthorhombicity (that is, lattice-constant ratio a/b) as a function of P concentration[72]. Although seemingly in line with the strong magnetostructural coupling discussed above, this result remains highly enigmatic owing to the apparent contradiction with first-order Landau theory, which forbids a linear relationship between these vector and scalar OPs. This strange but apparently universal coupling remains as an important topic in our understanding of the relationship between magnetism and structure in the FeAs-based materials.

Superconducting state — pairing symmetry

As for the high-T_c cuprates, the fundamental mechanism that causes the high-temperature superconductivity in the FeSCs is a question of primary importance. In both cases the experimental evidence so far favours an unconventional pairing mechanism closely tied to magnetism. Although the exact nature of the pairing is not known in either system at present, many experiments aimed to determine the pairing symmetry have been carried out. For the cuprates, the experimental evidence favours a singlet d-wave symmetry that involves a change in sign of the superconducting OP phase at nodal points situated at the Fermi energy (E_F) and directed along (π,π) in the simple 2D cuprate band structure. For the FeSCs, the initial measurements[31,73] probing the OP symmetry pointed to a fully gapped OP consistent with a fully symmetric s-wave symmetry. In comparison to cuprates and other magnetically mediated superconductors, this came as a surprise. However, the OP symmetry of FeSCs was in fact predicted theoretically to have s-wave symmetry, but with a sign change that occurs between different bands in the complex multiband electronic structure. This is the so-called $s\pm$ state, calculated before experiments[50] (see ref. 49 and Box 2 for more details), which will be predominantly discussed below in the context of experimental work.

Experiments that probe the symmetry of the SC phase provide important information about the energy and momentum dependence of Cooper pairing, and are therefore pivotal to helping elucidate the pairing mechanism in this new class of high-T_c superconductors. Owing to the vastness of the iron pnictide family and the nature of chemical substitution, one limitation so far is that many experiments have been carried out on different systems or different chemical compositions of the same crystalline system, and thus make comparisons difficult. However there is surprisingly good consistency, enabling general conclusions to be drawn from several experiments. For instance, NMR experiments were quick to determine from Knight shift measurements that the SC state spin symmetry is probably singlet[74–76], implying an even OP symmetry (that is, s wave, d wave and so on). So far, this experiment has been done on the main members of the FeSC family, including samples of the 1111- (refs 74,75), 122- (ref. 76) and 11-type (ref. 77) systems, so it is reasonable to assume that SC in the iron pnictides is universally spin singlet.

Determining the nature of the orbital OP symmetry, however, is much more complex and is at present the focus of most research. First, the much-discussed $s\pm$ state shares the same symmetry class as the simple s-wave case, reducing the number of available probes able to distinguish the two. Moreover, owing to the multi-orbital nature of the FeSCs and their nesting properties, anisotropic (extended) s- and d-wave states are nearly degenerate[78], making it difficult to identify the underlying symmetry even if experiments determine the presence of nodes in the gap function. Experiments to probe the orbital symmetry usually probe either the amplitude or the phase of the OP. For the cuprates, the phase experiments gave the most convincing evidence for a sign-changing d-wave ($d_{x^2-y^2}$) symmetry: corner junction tunnelling and SQUID experiments,

observation of half-integer flux quantum from polycrystalline materials or bicrystal *ab*-plane oriented films and absence of *c*-axis Josephson effect with an *s*-wave SC were all taken as evidence for *d*-wave symmetry.

For the FeSCs, only a few phase experiments have been done so far. In polycrystalline 1111 no half-integer flux was found by a scanning SQUID experiment[79], and a robust *c*-axis Josephson effect was found between Pb and K-doped $BaFe_2As_2$ (ref. 80), which rules out a predominant *d*-wave symmetry in these materials at the measured K concentrations. However, to distinguish a conventional *s*-wave state from $s\pm$ is not as straightforward as for a *d*-wave state. Several proposals for tunnelling/SQUID experiments have been made[81–83], but all require junction geometries more difficult to prepare than a simpler corner junction, and no experimental results have so far been reported. One new type of phase experiment has been reported[84], where half-integer flux quantum jumps were observed in a loop formed by Nb and polycrystalline $NdFeAsO_{0.88}F_{0.12}$. These jumps were interpreted as arising from π phase shifts at a few polycrystal boundaries as current is passed through the sample, which could only occur if the symmetry involves a sign-changing $s\pm$ state. A *d*-wave symmetry was ruled out because many more jumps would be expected in this case, and these were not observed by the scanning SQUID experiment[79]. Another phase-sensitive experiment, just reported[85] on a single crystal of Fe(Se, Te), uses spectroscopic-imaging scanning tunnelling microscopy to determine the sign of the OP gap by the magnetic-field dependence of the quasiparticle scattering strength. Because of the coherence factors, the scattering amplitudes are different for sign-changing and sign-constant symmetries. In Fe(Se, Te), it was found that the sign of the gap is reversed between the electron and hole pockets[85]. This, along with an absence of low-energy quasiparticle excitations in the tunnelling gap (as would be seen from the nodes in a *d*-wave SC), strongly suggests an $s\pm$ state. Together, all of these results favour the $s\pm$ state in the FeSCs, but definitive phase experiments on more materials are needed to conclusively settle the case.

Neutron scattering has been instrumental in helping clarify not only the magnetic properties[51], but also the interplay of magnetism and superconductivity in the FeSCs. For instance, strong evidence now exists for the competitive nature of AFM and SC coexistent phases in $BaFe_{2-x}Co_xAs_2$, as determined by the observation of a reduction of the static Fe moment on entering the SC state[52]. A systematic study of the same nature[86], comparing experimental results to a mean-field Ginsburg–Landau model, found this behaviour to be inconsistent with a non-sign-changing *s*-wave symmetry, providing further support for the $s\pm$ gap structure.

The observation of a collective magnetic-resonance mode that appears below the SC transition temperature is a well-known feature found by inelastic neutron-scattering experiments in cuprate, heavy-fermion and, most recently, FeSC compounds. This feature, which seems to universally relate the energy of the resonance mode to the SC energy gap[87], has now been clearly observed in superconducting 1111- (ref. 88), 122- (refs 89–92) and 11-type (refs 93,94) compounds, providing important implications for the symmetry of the OP (ref. 95). As shown in Fig. 2, the resonance observed in several experiments follows a very strong correlation with the SC state, as indicated by a scaling of the resonance energy with T_c. Because this relationship appears exclusively in nearly magnetic unconventional superconductors[87], it is considered either (optimistically) a strong signature of magnetically mediated pairing, or (pessimistically) an independent remnant of nearby magnetic order. In the first case, it is in fact possible to extract gap symmetry and phase information from the momentum dependence of the resonance by comparing with predictions for several differing gap symmetries[96]. In the second case, the resonance appears as a consequence of the

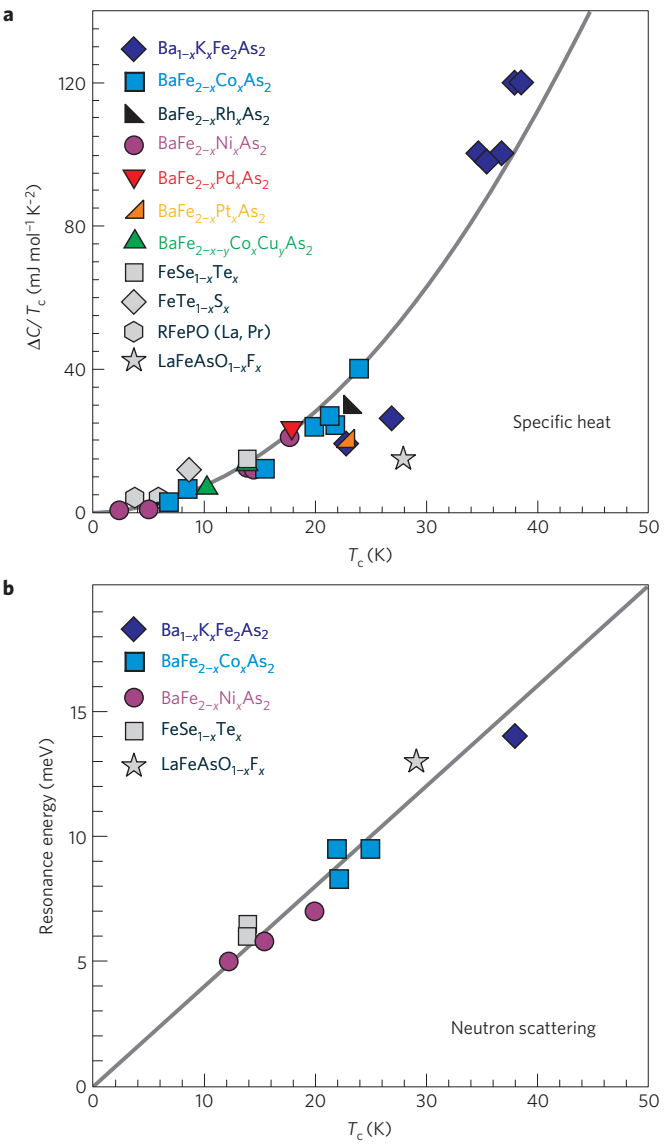

Figure 2 | Universal experimentally scalable quantities of FeAs-based superconducting materials. a, Absolute size of the measured jump in electronic specific heat at the superconducting transition in several members of 11-, 122- and 1111-type FeSC compounds plotted as a function of T_c. Originally identified in Co- and Ni-doped $BaFe_2As_2$ (ref. 122) and subsequently verified in K- (ref. 123), Co- (refs 115,124), Rh-, Pd- (ref. 125) and Pt-doped[12] $BaFe_2As_2$ systems, as well as $FeTe_{0.85}S_{0.15}$ (ref. 126), RFePO (refs 127,128), $FeSe_{0.5}Te_{0.5}$ (ref. 129) and $LaFeAsO_{0.89}F_{0.11}$ (ref. 130) superconductors, this thermodynamic quantity seems to scale quadratically with T_c in all cases, as demonstrated by the solid line fitted to a quadratic power law. **b**, Energy of magnetic neutron resonance measured at a commensurate (π,π) wave vector in several FeSC systems including 1111- (ref. 88), 122- (refs 89–92) and 11-type (refs 93,94) compounds, plotted as a function of T_c. The solid line is a linear fit to all data, indicating that the resonance energy scales linearly with T_c.

reduction of the rate of magnon decay through conduction electrons owing to the opening of the SC gap at T_c. Although the true relationship between the resonance and superconductivity remains unclear, these opposing scenarios can be delineated by experimental determination of any fine structure of the resonance mode. So far, neutron experiments carried out in high magnetic fields do not yet reveal any splitting[97]. Nonetheless, the striking observation of a resonance at the (π,π) nesting vector in $FeSe_{0.4}Te_{0.6}$

(ref. 93), despite the nearby magnetic order of FeTe that lives at a different ordering vector $(\pi, 0)$, provokes an interpretation that involves spin fluctuations at least circumstantially tied to superconductivity.

For amplitude-sensitive experiments, NMR experiments were the first to probe the OP symmetry by considering the temperature dependence of the nuclear relaxation rate $1/T_1$ below T_c, with a variety of results dominated by $\sim T^3$ behaviour (see refs 3,4), but with exceptions including much lower ($\sim T$) power laws consistent with a nodal OP structure in $BaFe_2As_{2-x}P_x$ and higher ($\sim T^5$) power laws more consistent with activated behaviour in $Ba_{1-x}K_xFe_2As_2$ (ref. 98). The intermediate ($\sim T^3$) power laws, although consistent with a 2D line-node model, could also be mimicking a crossover behaviour expected in a $s\pm$ gap model that accounts for disorder scattering, with exponential behaviour in $1/T_1$ expected only at low temperatures[95,99].

Measurements of thermal conductivity at temperatures approaching absolute zero are one of the best bulk-probe techniques for studying low-lying quasiparticle excitations in a superconductor, with the ability to provide strong constraints on the pairing symmetry. For a fully gapped single-band s-wave superconductor, the electronic thermal conductivity follows an activated behaviour in both temperature and field (H) dependence owing to the full gapping of the FS, going exponentially to zero with T and H for $T \ll T_c$ and $H \ll H_{c2}$ (with H_{c2} being the upper critical field). For a superconductor with nodes (see Box 2), a T-linear electronic component arises owing to residual nodal quasiparticle excitations induced by impurity scattering. Also, magnetic field is much more effective in activating thermal carriers, with the Volovik effect imposing a strong enhancement in nodal excitations that increases as $H^{1/2}$. In a multiband superconductor, particularly with the $s\pm$ structure, the exact expectation for thermal quantities is difficult to determine owing to the complex interplay of impurity, inter- and intra-band scattering, but has been addressed[100].

Several low-temperature thermal-conductivity measurements have now been reported for the FeSCs, with a variety of behaviours observed. Figure 3 presents a summary of the magnetic-field dependence of thermal conductivity measured in several Ba-based 122 compounds in the low-temperature ($T = 0$) limit, plotted as a function of reduced field to show both the T-linear component ($H = 0$ intercept) and the field dependence in the $T = 0$ limit[101–106]. As shown, even in this constrained set of compounds there is a widely varying set of behaviours, spanning the range between the standard fully gapped and nodal OP expectations described above. So far, this is one of the most puzzling results from OP symmetry-sensitive experiments: even within a controlled substitution series, such as in $BaFe_{2-x}Co_xAs_2$, there is a strong evolution of the field enhancement of thermal carriers with doping, suggestive of an evolution of the gap structure[102]. Even more perplexing is the fact that, in contrast to Co- and Ni-doped $BaFe_2As_2$, a T-linear term is observable in $BaFe_2(As_{0.67}P_{0.32})_2$ (ref. 106), signifying that the development of nodes in the gap structure is sensitive to the type of chemical substitution. Furthermore, the 'extremely overdoped' stoichiometric compound KFe_2As_2 also seems to show low-energy excitations consistent with line nodes[105], as opposed to $Ba_{1-x}K_xFe_2As_2$ near optimal K concentration[101].

However, this apparently confusing situation may be consistent with the proposed $s\pm$ gap structure due to the development of accidental nodes (or at least deep minima) in the OP under certain conditions.

For instance, it has been shown theoretically that disorder can 'lift' existing nodes in an $s\pm$ OP owing to the averaging of anisotropy by intraband scattering[107]. It was also suggested that nodes can appear when a third hole pocket at (π, π) is absent, or more generally when variations in the electronic structure are imposed by its sensitivity to the Fe–As tetrahedral bond geometry.

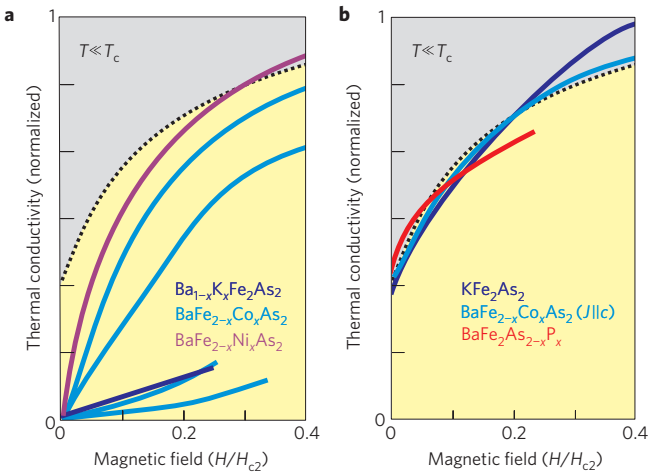

Figure 3 | Electronic thermal conductivity of FeAs-based systems in the superconducting state. a,**b**, Thermal-conductivity data in the $T = 0$ limit of several members of the chemically substituted $BaFe_2As_2$ family are plotted normalized to normal-state values (that is, at H_{c2}) as a function of applied field normalized to upper-critical-field values. Experimental data sets include $Ba_{1-x}K_xFe_2As_2$ (ref. 101), KFe_2As_2 (ref. 105), $BaFe_{2-x}Co_xAs_2$ for basal plane[102] and c-axis current orientations[108], $BaFe_{2-x}Ni_xAs_2$ (ref. 104) and $BaFe_2As_{2-x}P_x$ (ref. 106). These are separated for clarity purposes into data sets that do not exhibit a residual (that is, y-intercept) contribution attributable to low-energy quasiparticle excitations at zero field (**a**) and data sets that do show a clear residual contribution at zero field (**b**). Note that all systems that exhibit a residual contribution (right) also show exceptionally similar field dependence, closely following the expectation for an unconventional superconductor with line nodes in its gap symmetry (dotted lines).

For instance, it is claimed that the tendency towards magnetism becomes stronger with increasing pnictogen height above the Fe plane, causing multiple spin-fluctuation modes to conspire to result in either a fully gapped OP or one with nodes[28].

Both the temperature and field dependencies of thermal conductivity have been calculated for several combinations of two-band s-wave symmetries, including non-sign-changing and sign-changing cases with anisotropies and varying rates of disorder scattering imposed[100]. A plethora of expectations are found, from fully activated behaviour in an isotropic two-gap (s_{++} or $s\pm$) state with no disorder to a finite non-universal residual electronic term in an anisotropic two-gap ($s\pm$) state that depends non-monotonically on disorder. A strong field dependence at small H rules out a clean $s\pm$ state for 122-type materials but is consistent with pair-breaking scattering. However, the pair-breaking would have to be unphysically strong (note that $Ba_{1-x}K_xFe_2As_2$ and $BaFe_{2-x}Co_xAs_2$ probably have very different levels of disorder owing to ion-replacement location). Therefore, the conclusion is that the 122-type materials probably have a multiband A_{1g} (s-wave) symmetry state with a highly anisotropic gap on one FS (ref. 100). Although this seems to be inconsistent with ARPES experiments, which so far show only isotropic gap structures[30,31,55], the situation may be reconciled in a scenario where the SC OP has a strong 3D momentum dependence. In particular, very recent thermal conductivity experiments on $BaFe_{2-x}Co_xAs_2$ in the zero-temperature limit have uncovered a finite residual T-linear component when thermal currents are directed along the crystallographic c axis[108], which is consistent with the presence of nodes on part of the FS. Because the normalized (relative to the normal state) residual conductivity quickly rises for both current directions with field and even becomes isotropic at ~25% of H_{c2}, a scenario where an effectively 2D FS harbours a gap

with non-zero minima and a more 3D surface (that is warped enough to contribute to c-axis transport) harbours a gap with nodes is suggested[108]. Although the experiment cannot distinguish between a structure with nodes positioned at zero- or finite-valued $\mathbf{k_z}$, theoretical predictions for a proximity-induced gap would be consistent with c-axis nodes[109]. What is most striking, however, is that the residual conductivity is most pronounced away from optimal doping, which is either an extrinsic effect due to an impurity- or disorder-induced normal-state contribution (possibly related to the residual heat capacity discussed below), or an intrinsic signature of the nature of the SC gap. As pointed out in ref. 108, 'modulation is a sign of weakness', which translates to the provocative idea that deviations from two-dimensionality may weaken the SC state in the iron pnictides. Nevertheless, future experiments should help settle these issues. Specifically, magnetic-field angle-resolved thermal-conductivity and specific-heat studies should delineate the position(s) of nodes and the OP symmetry. Recent specific-heat measurements on the related material $Fe_{1+x}Se_{0.4}Te_{0.6}$ have indeed revealed a four-fold oscillation in the basal plane consistent with either nodes or deep minima in the gap structure[110].

Temperature-dependent penetration-depth experiments have also given a wide disparity of results, including activated (exponential) behaviour in $PrFeAsO_{1-y}$ and $SmFeAsO_{1-x}F_y$, and power-law behaviour in 1111- and 122-type FeSCs and in chalcogenide- and phosphide-based systems (see ref. 4 for detailed references). These variations can possibly be explained as due to impurities or other disorder, because the T dependence of the penetration depth is very sensitive to disorder and paramagnetic contributions. This was shown systematically in the 122 system, where the exact temperature dependence was shown to vary as a function of intrinsic disorder in the case of $Ba_{1-x}K_xFe_2As_2$ (ref. 111) and as a function of disorder imposed by irradiation in the case of Co- and Ni-doped $BaFe_2As_2$ (ref. 112). Also, the activated behaviour in Pr- and Sm-based 1111-type materials is put into question in a study on La- and Nd-based 1111-type crystals[113], where the subtraction of a paramagnetic contribution reveals a quadratic temperature dependence of the London penetration depth. These corrected data can be fitted with a two-gap s-wave model, but issues with the extracted $\mathbf{\Delta}/k_BT_c$ ratios being smaller than the Bardeen–Cooper–Schrieffer (BCS) expectations and deviations of the fits near T_c call for a model that considers interband scattering in more detail. Another example of a two-gap fit is shown with a local measurement of penetration depth in Ba $(Fe_{0.95}Co_{0.05})_2As_2$ using magnetic force microscopy and scanning SQUID spectroscopy, which observed a temperature dependence that varies about ten times more slowly than in bulk measurements[114]. These data were well fitted with a fully gapped model with two different gaps, whereas the bulk measurement is not obviously consistent with a fully gapped model unless disorder is considered.

Recent studies of the low-temperature electronic specific heat (γ) have added important insights. In the $BaFe_{2-x}Co_xAs_2$ system, a systematic study of the SC portion of γ as a function of x has revealed a lack of any strong doping dependence, signifying no major change in the gap structure through the superconducting range of concentrations; the data of ref. 115 are fitted using a two-gap model, yielding a factor-of-two ratio between gap amplitudes that does not vary by more than 10% through several Co concentrations. The width of the SC transition at T_c, however, does show a significant increase away from optimal doping. This may be in line with the conclusions from thermal-conductivity measurements of weakened pairing strength away from optimal doping[108]. A more intriguing find involves measurements of γ in the $T = 0$ limit in $Ba(Fe_{0.92}Co_{0.08})_2As_2$ ($T_c = 20$ K; ref. 115) and $BaFe_2(As_{0.7}P_{0.3})_2$ ($T_c = 30$ K; ref. 116), both of which report a sizeable residual contribution in the SC state that is ~20% of the estimated normal-state electronic contribution. However, subsequent studies have shown this residual contribution to be minimized at optimal doping in $BaFe_{2-x}Co_xAs_2$ (ref. 117), and vanishingly small in $Ba_{0.68}K_{0.32}Fe_2As_2$ (refs 118,119), pointing to an origin linked to sample homogeneity. Although unconventional, the field dependence of γ in both FeSC systems does not follow the usual behaviour expected for nodal excitations, such as the well-known $H^{1/2}$ dependence due to the Volovik effect. In $Ba(Fe_{0.92}Co_{0.08})_2As_2$, a sublinear field dependence is indeed present but it cannot be fitted by a clean d-wave gap, and is better described by either a dirty d-wave or an anisotropic s-wave gap structure[115]. Likewise, in $BaFe_2(As_{0.7}P_{0.3})_2$ (ref. 116) and $Ba_{0.6}K_{0.4}Fe_2As_2$ (ref. 120) the observed linear field dependence is more in line with a pairing symmetry that is isotropic on at least one FS sheet that contributes significantly to the electronic density of states (ref. 116). However, a recent calculation of the Volovik effect for a two-band s-wave state with unequal gap sizes does suggest that deviations from the usual square-root dependence are not unexpected[121].

A more provocative observation has to do with an unusual scaling of the jump in specific heat with T_c, as first identified in K-, Co- and Ni-doped $BaFe_2As_2$ systems[122]. Because the phonon contribution is difficult to estimate near T_c owing to elevated temperatures, it is not straightforward to extract the electronic normal state γ at the transition and thus enable a comparison of the usual normalized ratio $\Delta C(T_c)/\gamma T_c$ to the BCS expectation of 1.43. Instead, ref. 122 compared the absolute size of the jump, $\Delta C(T_c)$, and T_c values of several different samples and found a unique power-law scaling that seems to go as $\Delta C(T_c) \sim T_c^3$. As shown in Fig. 3, a compilation of all data available for FeSC systems so far confirms the initial observation to hold in subsequent measurements of K-doped[118,119,123] and Co-doped[115,124] $BaFe_2As_2$ systems. Measurements in several other systems, including Rh-, Pd- (ref. 125) and Pt-doped[12] $BaFe_2As_2$ materials, as well as $FeTe_{0.85}S_{0.15}$ (ref. 126), LaFePO (ref. 127), PrFePO (ref. 128), $FeSe_{0.5}Te_{0.5}$ (ref. 129) and $LaFeAsO_{0.89}F_{0.11}$ (ref. 130), also fall approximately on the scaling plot. (Note that, so far, 1111-type FeSCs rarely show a large signature of their SC transitions in specific heat, possibly due to sample quality, which may be improved in the future.) Assuming that the enhancement $\Delta C(T_c)$ is purely electronic, this observation is difficult to explain using BCS theory. According to ref. 131, it would require extremely unnatural fine-tuning of the pairing attraction to attain the proper scaling, leading to the conclusion that the underlying ground state is not a usual Fermi liquid but instead is quantum critical. However, it has also been proposed that strong pair-breaking can also result in such scaling[132]. These opposing views can potentially be explained through controlled studies of specific heat and pair-breaking, the latter being discussed below.

First noted in the case of $SrFe_{2-x}Co_xAs_2$ (ref. 10), it was quickly recognized that the act of chemical substitution directly into the active pairing layer in the FeSCs presents a stunning contrast to the well-known detrimental effect of Cu-plane disorder in the cuprates. Although there is a consensus that it is better (in the sense of attaining higher T_c values) to minimize disorder within the Fe planes, the mere fact that we can still attain a T_c value near 25 K with strong disorder in the Fe plane (that is, by ~10% substitution for Fe) presents a conundrum: how do we disentangle the good (doping/SC optimization) from the bad (pair-breaking disorder)? Pair-breaking studies are extremely useful for identifying a sign-changing OP, where non-magnetic impurities should be strong pair-breakers owing to the effect of a scattering event on the momentum-coupled OP phase. However, given the debate about the effects of chemical substitution in FeSCs discussed earlier, it is not clear how any substitution within the active layer can be

considered to act only as an impurity scattering centre. Luckily, there are other methods of systematically inducing disorder. For example, alpha-particle irradiation was used to study pair-breaking in a controlled manner by irradiating a $NdFeAsO_{1-x}F_x$ single-crystal sample with $T_c(0) = 46$ K (ref. 133), resulting in a weak suppression of T_c closely tied to irradiation-induced defects of a magnetic nature. This is suggestive of a sign-changing OP. Penetration-depth measurements of Co- and Ni-doped $BaFe_2As_2$ as a function of irradiation with Pb ions have also shown a 'clean' suppression of T_c with increasing defects, as well as a systematic suppression of the low-temperature power-law exponent of the penetration-depth temperature dependence that is consistent with a nodeless $s\pm$ state affected by pair-breaking scattering intermediate between Born and unitary limits[112].

Finally, results from other experiments provide further insight that must be considered. Raman scattering is particularly useful because it is capable of sampling specific regions of the BZ, hence probing the momentum distribution of low-lying gap excitations. A Raman study on $BaFe_{2-x}Co_xAs_2$ samples[134] provides evidence for a strong gap variation on the electron pockets consistent with the anisotropic $s\pm$ state discussed above. Muon spin-relaxation measurements of the penetration depth of optimally doped $Ba(Fe_{0.926}Co_{0.074})_2As_2$ fit well to an isotropic two-gap structure with one of the gaps being very small as compared with the BCS expectation[135]. Last but not least, scanning tunnelling microscopy experiments on $BaFe_{2-x}Co_xAs_2$ have revealed an unusual gap structure that does not strictly fit either a simple s- or d-wave shape, but also does not show any fourfold internal vortex structure that would be expected in a d-wave case[136]. Such direct measures of the superconducting OP symmetry will be important for future determination of the true variety of gap structures in the FeSC materials.

Pairing mechanism, correlations and quantum criticality

From a general standpoint, the interplay of magnetism and superconductivity strongly suggests that magnetic fluctuations are involved either directly or indirectly in the Cooper pairing in the FeSCs. In the context of magnetism, pairing could arise from fluctuations emanating from a quantum critical point, or an alternative pairing mechanism may simply benefit from the suppression of an antagonistic long-range magnetically ordered state, or a more complicated scenario involving the optimal combination of three players — Coulomb repulsion, spin fluctuations and phonon coupling — may favour high-T_c superconductivity in these materials. First off, phonons alone were quickly ruled out as a standalone contender for the pairing mediator. A calculation of electron–phonon coupling from first principles helped to conclude that LaFeAsOF is intrinsically at most a very poor electron–phonon superconductor (although including the effects of magnetism can increase the coupling constant by up to 50%; ref. 137). The classic isotope-effect experiment, which provided the first strong evidence for phonon-mediated Cooper pairing in conventional superconductors, is a well-known method of probing the role of phonons (albeit not always conclusively even for conventional superconductors). One of the first studies did not find any O isotope effect in $SmFeAsO_{1-x}F_x$, but did find a significant Fe isotope effect ('α' exponent of ~0.35) on both the magnetic and superconducting transitions in both $SmFeAsO_{1-x}F_x$ and $Ba_{1-x}K_xFe_2As_2$ (ref. 138), suggesting that phonons are at least intermediate players. However, subsequent studies on control- and isotope-substituted samples of both systems grown under identical conditions report the absence of an appreciable isotope effect in either case, motivating the need for further study[139].

The strength of the electronic correlations in the iron-based materials is an important issue that has received much theoretical and experimental study. The present experiments show that a modest level of correlations exists, but that the correlations are not as strong as in the cuprates. A simple indication of this is the absence of any clear Mott physics in the FeSCs: the parent compounds are all clearly metallic, and there is no indication of nearby insulating behaviour. However, conflicting opinions have been generated by experimental results. Optical measurements on LaFePO have indicated that many-body effects are important, identifying this material as a moderately correlated metal and $BaFe_2As_2$ as even more so[140]. In contrast, X-ray absorption and inelastic scattering measurements on $SmFeAsO_{0.85}$, $BaFe_2As_2$ and $LaFe_2P_2$ show that their spectra closely resemble those of elemental metallic Fe, thus arguing for weak correlations in these materials[141] (although elemental Fe itself, with a Curie temperature of over 1,000 K, is not exactly an uncorrelated system!). Recent calculations indicate that the correlated nature of the paramagnetic state gives rise to very fast-fluctuating moments[142], providing a potential explanation for the reduced static moment size observed experimentally. In the end, LaFePO may indeed have stronger correlations than 1111- and 122-type FeSC materials, which could explain the observations of more unconventional (possibly d-wave) superconductivity in this system.

Regardless of the role of strong correlations, spin fluctuations, which possibly provide the collective spin-one excitation that mediates pairing, are clearly abundant in the FeSCs. Considering the first-order nature of the SDW transitions in these systems, the fluctuations are surprisingly persistent up to fairly high temperatures. For instance, the well-known increasing behaviour of magnetic susceptibility up to very high temperatures, so far a universal feature of the FeSCs, is considered an indication of AFM fluctuations[143]. Also, Mossbauer spectroscopy of $BaFe_{2-x}Co_xAs_2$ has observed a magnetic hyperfine component consistent with short-range AFM correlations at temperatures up to $1.5 \times T_N$ (ref. 144), and neutron-scattering studies of $CaFe_2As_2$ provide evidence for 2D spin fluctuations that persist up to $1.8 \times T_N$ (ref. 145) — all despite the first-order nature of both magnetic and structural transitions in these systems.

An NMR study of normal-state spin dynamics in $BaFe_{2-x}Co_xAs_2$ has shown that the uniform spin susceptibility is systematically suppressed with increasing Co concentration, with superconductivity optimized near a quantum critical point where SDW order spin fluctuations are maximal[146]. This was suggested to be controlled by the suppression of inter-band transitions (that is, disappearance of a hole pocket) that weakens the nesting condition[49], and it is indeed true that dHvA oscillations observed in the related P-doped $BaFe_2As_2$ system show a substantial shrinking of electron pockets and strong mass enhancement on approach to the magnetic/superconducting boundary at optimal T_c (ref. 32). Because the measured Fermi surfaces in the P-doped series are inconsistent with an estimated (extrapolated) smooth progression between P and As end-members, it was concluded in ref. 32 that spin fluctuations are the likely explanation for band structure changes, and consequentially superconductivity.

With good ties between superconductivity and spin fluctuations from the suppression of magnetic order, it is fair to say that quantum criticality may play an important role. Calculations indeed suggest a competition between electron localization and itinerancy, which should yield fertile soil for quantum criticality[147], and the observed specific heat scaling as noted above may provide strong evidence for a truly non-Fermi-liquid ground state[131]. However, experimentally there is surprisingly little evidence for strong deviations from Fermi-liquid behaviour, especially as compared with other quantum critical systems such as the cuprates and heavy-fermion materials. For example, although T-linear resistivity is indeed rampant throughout the optimally doped FeSCs, disentanglement of electron and hole carriers (with some assumptions) has enabled transport measurements

of $BaFe_{2-x}Co_xAs_2$ to be interpreted as consistent with Fermi-liquid expectations[46]. More importantly, strong evidence for a Fermi-liquid ground state in $BaFe_2As_{2-x}P_x$ is provided directly by the observation of quantum oscillations throughout its phase diagram[32], even though this system's normal state above T_c shows tell-tale signatures of a quantum critical point near $x = 0.66$ (ref. 148). Because transport measurements near optimal doping are limited to temperatures above T_c, it will be an experimental task to develop methods of probing the low-temperature ground state either indirectly in SC systems, or by studying related low-T_c or non-SC materials that can be tuned to criticality, to explain the true ground-state properties near the demise of AFM order. Recent progress has been made to this effect, for instance in Cu-doped $BaFe_2As_2$ (ref. 15) and P-doped CeFeAsO (ref. 72), both of which show complete suppression of magnetic order in the absence of any SC phase.

With difficulties in probing the underlying ground state near the quantum critical point, studies of the coexistence region of superconductivity and antiferromagnetism are among the most important ongoing efforts. Muon spin-resonance experiments have shown contrasting pictures regarding the level of coexistence, with a complete separation of AFM and SC phases shown in studies of La- and Ce-based 1111-type materials[5] and coexistence of disordered but static magnetism and superconductivity in SmFeAsOF with possible phase separation[6]. In the 122-type materials, mesoscopic phase separation into magnetic and paramagnetic (superconducting) regions has been shown in $Ba_{1-x}K_xFe_2As_2$, $Sr_{1-x}Na_xFe_2As_2$ and $CaFe_2As_2$ under pressure[149]. If experiments can show that microscopic coexistence of AFM and SC is indeed intrinsic to FeSC systems, then the competition of these two ground states is not surprising in a scenario where Cooper pairing is mediated by strong fluctuations of AFM order. This is indeed the case in the Ce-based 115-type materials, where the same f-electron states are known to be responsible for both AFM and SC. A recent report[150] of 'atomic' coexistence of SC and AFM order on each Fe site is a thought-provoking observation that speaks to the level at which these two states of matter can cohabitate.

Conclusions

Progress in understanding superconductivity in iron-based materials has advanced tremendously over the past year thanks to abundant theoretical and experimental efforts. Considering that there is overall good agreement between many different experiments on the general properties of these materials, we can safely conclude that the chemistry is under sufficient control to allow for reasonable comparisons of experimental data without major concerns about sample quality variations. This is one of the main reasons why, after only two years, we have an extensive and reliable set of thermodynamic, transport, surface and spectroscopic data with which to analyse the general and universal properties of this new breed of superconductors. It is also the reason why the observed diversity of properties, especially of the SC state, is so puzzling: the intrinsic nature of these materials seems to include a strong sensitivity to many real and unavoidable perturbations, which yields diverse yet reproducible results. Theoretically, this may be due to a near degeneracy in energy of different extended s-wave and even d-wave OP symmetry states, implying a sensitivity of gap symmetry to everything from disorder to lattice density. Overall, it is likely that a generic representative OP symmetry will involve a sign-changing structure with one fairly isotropic gap and another gap with at least deep minima, and more probably with accidental nodes. In particular, the presence of anisotropic and multiband scattering, and strong c-axis dispersion of at least parts of the FS structure, will make it difficult to conclude on any particular universal gap structure. However, phase-sensitive experiments will help to pin down an intrinsic symmetry, and controlled experiments designed to probe the accidental nature of nodes may provide a better understanding of their dependence on tunable experimental quantities. In the end, these may be moot points, as the relatively high T_c values of the iron-based superconductors do not seem to care much about such details.

Finally, this brief review article cannot hope to cover all of the ongoing research in such an active and rapidly developing field as the iron-based superconductors. For example, the possible role of more exotic physics, such as nematic order, has not been discussed. Also, the physics and experiments related to possible applications of these materials, especially those involving the significantly high values of upper critical fields of the order of 50 T and critical currents exceeding $10^6\,A\,cm^{-2}$, have been omitted. The research on the FeSCs has already led to new insights into the novel physics of correlated electronic materials, but there is still much to learn. If the cause of the high-temperature superconductivity in these materials can be understood at the level that conventional electron–phonon superconductors are understood, then it is possible that room-temperature superconductivity may prove feasible. Even if this elusive goal is not achieved, the future research on iron-based systems will lead to more knowledge of materials with exotic condensed-matter-physics properties. As has already been shown by the iron-based superconductors, the cuprates, the organics and the heavy fermions, superconductivity and magnetism are not as incompatible as was once believed.

References

1. Kamihara, Y., Watanabe, T., Hirano, M. & Hosono, H. Iron-based layered superconductor $La[O_{1-x}F_x]FeAs$($x = 0.05$–0.12) with $T_c = 26$ K. *J. Am. Chem. Soc.* **130,** 3296–3297 (2008).
2. Takahashi, H. *et al.* Superconductivity at 43 K in an iron-based layered compound $LaO_{1-x}F_xFeAs$. *Nature* **453,** 376–378 (2008).
3. Ishida, K., Nakaii, Y. & Hosono, H. To what extent iron-pnictide new superconductors have been clarified: A progress report. *J. Phys. Soc. Jpn* **78,** 062001 (2009).
4. Johnston, D. C. The puzzle of high temperature superconductivity in layered iron pnictides and chalcogenides. Preprint at http://arxiv.org/abs/1005.4392.
5. Luetkens, H. *et al.* The electronic phase diagram of the $LaO_{1-x}F_xFeAs$ superconductor. *Nature Mater.* **8,** 305–309 (2009).
6. Drew, A. J. *et al.* Coexistence of static magnetism and superconductivity in $SmFeAsO_{1-x}F_x$ as revealed by muon spin rotation. *Nature Mater.* **8,** 310–314 (2009).
7. Rotter, M., Pangerl, M., Tegel, M. & Johrendt, D. Superconductivity and crystal structures of $(Ba_{1-x}K_x)Fe_2As_2$ ($x = 0$–1). *Angew. Chem. Int. Ed.* **47,** 7949–7952 (2008).
8. Ni, N. *et al.* Effects of Co substitution on thermodynamic and transport properties and anisotropic H_{c2} in $Ba(Fe_{1-x}Co_x)_2As_2$ single crystals. *Phys. Rev. B* **78,** 214515 (2008).
9. Jiang, S. *et al.* Superconductivity up to 30 K in the vicinity of the quantum critical point in $BaFe_2(As_{1-x}P_x)_2$. *J. Phys. Condens. Matter* **21,** 382203 (2009).
10. Leithe-Jasper Schnelle, W., Geibel, C. & Rosner, H. Superconducting state in $SrFe_{2-x}Co_xAs_2$ by internal doping of the iron arsenide layers. *Phys. Rev. Lett.* **101,** 207004 (2008).
11. Sefat, A. S. *et al.* Superconductivity at 22 K in Co-doped $BaFe_2As_2$ crystals. *Phys. Rev. Lett.* **101,** 117004 (2008).
12. Saha, S. R. *et al.* Superconductivity at 23 K in Pt doped $BaFe_2As_2$ single crystals. *J. Phys. Condens. Matter* **22,** 072204 (2010).
13. Sefat, A. S. *et al.* Absence of superconductivity in hole-doped $BaFe_{2-x}Cr_xAs_2$ single crystals. *Phys. Rev. B* **79,** 224524 (2009).
14. Liu, Y., Sun, D. L., Park, J. T. & Lin, C. T. Aliovalent ion-doped $BaFe_2As_2$: Single crystal growth and superconductivity. *Physica C* doi:10.1016/j.physc.2009.11.024 (2009).
15. Canfield, P. C., Bud'ko, S. L., Ni, N., Yan, J. Q. & Kracher, A. Decoupling of the superconducting and magnetic/structural phase transitions in electron-doped $BaFe_2As_2$. *Phys. Rev. B* **80,** 060501(R) (2009).
16. Kimber, S. A. J. *et al.* Similarities between structural distortions under pressure and chemical doping in superconducting $BaFe_2As_2$. *Nature Mater.* **8,** 471–475 (2009).
17. Alireza, P. L. *et al.* Superconductivity up to 29 K in $SrFe_2As_2$ and $BaFe_2As_2$ at high pressures. *J. Phys. Condens. Matter* **21,** 012208 (2009).

18. Colombier, E., Bud'ko, S. L., Ni, N. & Canfield, P. C. Complete pressure-dependent phase diagrams for $SrFe_2As_2$ and $BaFe_2As_2$. *Phys. Rev. B* **79,** 224518 (2009).
19. Ishikawa, F. *et al.* Zero-resistance superconducting phase in $BaFe_2As_2$ under high pressure. *Phys. Rev. B* **79,** 172506 (2009).
20. Fukazawa, H. *et al.* Suppression of magnetic order by pressure in $BaFe_2As_2$. *J. Phys. Soc. Jpn* **77,** 105004 (2008).
21. Matsubayashi, K. *et al.* Intrinsic properties of AFe_2As_2 (A = Ba, Sr) single crystal under highly hydrostatic pressure conditions. *J. Phys. Soc. Jpn* **78,** 073706 (2009).
22. Yamazaki, T *et al.* Appearance of pressure-induced superconductivity in $BaFe_2As_2$ under hydrostatic conditions and its extremely high sensitivity to uniaxial stress. *Phys. Rev. B* **81,** 224511 (2010).
23. Yu, W. *et al.* Absence of superconductivity in single-phase $CaFe_2As_2$ under hydrostatic pressure. *Phys. Rev. B* **79,** 020511R (2009).
24. Yildirim, T. Strong coupling of the Fe-spin state and the As–As hybridization in iron-pnictide superconductors from first-principle calculations. *Phys. Rev. Lett.* **102,** 037003 (2009).
25. Saha, S. R., Butch, N. P., Kirshenbaum, K., Paglione, J. & Zavalij, P. Y. Superconducting and ferromagnetic phases induced by lattice distortions in stoichiometric $SrFe_2As_2$ single crystals. *Phys. Rev. Lett.* **103,** 037005 (2009).
26. Kalisky, B. *et al.* Enhanced superfluid density on twin boundaries in $Ba(Fe_{1-x}Co_x)_2As_2$. *Phys. Rev. B* **81,** 184513 (2010).
27. Singh, D. J. Electronic structure of Fe-based superconductors. *Physica C* **469,** 418–424 (2009).
28. Kuroki, K., Usui, H., Onari, S., Arita, R. & Aoki, H. Pnicogen height as a possible switch between high-T_c nodeless and low-T_c nodal pairings in the iron-based superconductors. *Phys. Rev. B* **79,** 224511 (2009).
29. Lu, D. H. *et al.* Electronic structure of the iron-based superconductor LaOFeP. *Nature* **455,** 81–84 (2008).
30. Kondo, T. *et al.* Momentum dependence of the superconducting gap in $NdFeAsO_{0.9}F_{0.1}$ single crystals measured by angle resolved photoemission spectroscopy. *Phys. Rev. Lett.* **101,** 147003 (2008).
31. Ding, H. *et al.* Observation of Fermi-surface-dependent nodeless superconducting gaps in $Ba_{0.6}K_{0.4}Fe_2As_2$. *Europhys. Lett.* **83,** 47001 (2008).
32. Shishido, H. *et al.* Evolution of the Fermi surface of $BaFe_2(As_{1-x}P_x)_2$ on entering the superconducting dome. *Phys. Rev. Lett.* **104,** 057008 (2010).
33. Harrison, N. *et al.* Quantum oscillations in antiferromagnetic $CaFe_2As_2$ on the brink of superconductivity. *J. Phys. Condens. Matter* **21,** 32220 (2009).
34. Singh, D. J. Electronic structure and doping in $BaFe_2As_2$ and LiFeAs: Density functional calculations. *Phys. Rev. B* **78,** 094511 (2008).
35. Utfeld, C. *et al.* Bulk electronic structure of optimally doped $Ba(Fe_{1-x}Co_x)_2As_2$. *Phys. Rev. B* **81,** 064509 (2010).
36. Sekiba, Y. *et al.* Electronic structure of heavily electron-doped $BaFe_{1.7}Co_{0.3}As_2$ studied by angle-resolved photoemission. *New J. Phys.* **11,** 025020 (2009).
37. Liu, C. *et al.* K-doping dependence of the Fermi surface of the iron–arsenic $Ba_{1-x}K_xFe_2As_2$ superconductor using angle-resolved photoemission spectroscopy. *Phys. Rev. Lett.* **101,** 177005 (2008).
38. Brouet, V. *et al.* Nesting between hole and electron pockets in $Ba(Fe_{1-x}Co_x)_2As_2$ ($x = 0$–0.3) observed with angle-resolved photoemission. *Phys. Rev. B* **80,** 165115 (2009).
39. Kasahara, S. *et al.* Evolution from non-Fermi to Fermi liquid transport properties by isovalent doping in $BaFe_2(As_{1-x}P_x)_2$ superconductors. *Phys. Rev. B* **81,** 184519 (2010).
40. Rullier-Albenque, F., Colson, D., Forget, A., Thuery, P. & Poissonne, S. Hole and electron contributions to the transport properties of $Ba(Fe_{1-x}Ru_x)_2As_2$ single crystals. *Phys. Rev. B* **81,** 224503 (2010).
41. Wadati, H., Elfimov, I. & Sawatzky, G. A. Where are the extra d electrons in transition-metal substituted Fe pnictides? Preprint at http://arxiv.org/abs/1003.2663 (2010).
42. Liu, C. *et al.* Evidence for a Lifshitz transition in electron-doped iron arsenic superconductors at the onset of superconductivity. *Nature Phys.* **6,** 419–423 (2010).
43. Liu, C. *et al.* Three- to two-dimensional transition of the electronic structure in $CaFe_2As_2$: A parent compound for an iron arsenic high-temperature superconductor. *Phys. Rev. Lett.* **102,** 167004 (2009).
44. Malaeb, W. *et al.* Three-dimensional electronic structure of superconducting iron pnictides observed by angle-resolved photoemission spectroscopy. *J. Phys. Soc. Jpn* **78,** 123706 (2009).
45. Mun, E. D., Bud'ko, S. L., Ni, N., Thaler, A. N. & Canfield, P. C. Thermoelectric power and Hall coefficient measurements on $Ba(Fe_{1-x}T_x)_2As_2$ (T = Co and Cu). *Phys. Rev. B* **80,** 054517 (2009).
46. Rullier-Albenque, F., Colson, D., Forget, A. & Alloul, H. Hall effect and resistivity study of the magnetic transition, carrier content, and Fermi-liquid behavior in $Ba(Fe_{1-x}Co_x)_2As_2$. *Phys. Rev. Lett.* **103,** 057001 (2009).
47. Lee, C-H. *et al.* Effect of structural parameters on superconductivity in fluorine-free $LnFeAsO_{1-y}$ (Ln = La, Nd). *J. Phys. Soc. Jpn* **77,** 083704 (2008).
48. Gooch, M. *et al.* Superconductivity in ternary iron pnictides: AFe_2As_2 (A = alkali metal) and LiFeAs. *Physica C* doi:10.1016/j.physc.2009.10.096 (2009).
49. Mazin, I. I. & Schmalian, J. Pairing symmetry and pairing state in ferropnictides: Theoretical overview. *Physica C* **469,** 614–623 (2009).
50. Mazin, I. I., Singh, D. J., Johannes, M. D. & Du, M. H. Unconventional superconductivity with a sign reversal in the order parameter of $LaFeAsO_{1-x}F_x$. *Phys. Rev. Lett.* **101,** 057003 (2008).
51. Lynn, J. W. & Dai, P. Neutron studies of the iron-based family of high T_c magnetic superconductors. *Physica C* **469,** 469–476 (2009).
52. Lumsden, M. D. & Christianson, A. D. Magnetism in Fe-based superconductors. *J. Phys. Condens. Matter* **22,** 203203 (2010).
53. Yildirim, T. Origin of the 150-K anomaly in LaFeAsO: Competing antiferromagnetic interactions, frustration, and a structural phase transition. *Phys. Rev. Lett.* **101,** 057010 (2008).
54. Hu, W. Z. *et al.* Origin of the spin density wave instability in AFe_2As_2 (A = Ba, Sr) as revealed by optical spectroscopy. *Phys. Rev. Lett.* **101,** 257005 (2008).
55. Terashima, K. *et al.* Fermi surface nesting induced strong pairing in iron-based superconductors. *Proc. Natl Acad. Sci. USA* **106,** 7330–7333 (2010).
56. Coldea, A. I. *et al.* Fermi surface of superconducting LaFePO determined from quantum oscillations. *Phys. Rev. Lett.* **101,** 216402 (2008).
57. Analytis, J. G., Chu, J-H., McDonald, R. D., Riggs, S. C. & Fisher, I. R. Enhanced Fermi surface nesting in superconducting $BaFe_2(As_{1-x}P_x)_2$ revealed by de Haas–van Alphen effect. Preprint at http://arxiv.org/abs/1002.1304 (2010).
58. Qiu, Y. *et al.* Spin gap and resonance at the nesting wave vector in superconducting $FeSe_{0.4}Te_{0.6}$. *Phys. Rev. Lett.* **103,** 067008 (2009).
59. Yi, M. *et al.* Unconventional electronic reconstruction in undoped $(Ba, Sr)Fe_2As_2$ across the spin density wave transition. *Phys. Rev. B* **80,** 174510 (2009).
60. Eremin, I. & Chubukov, A. V. Magnetic degeneracy and hidden metallicity of the spin-density-wave state in ferropnictides. *Phys. Rev. B* **81,** 024511 (2010).
61. Cvetkovic, V. & Tesanovic, Z. Multiband magnetism and superconductivity in Fe-based compounds. *Europhys. Lett.* **85,** 37002 (2009).
62. Diallo, S. O. *et al.* Itinerant magnetic excitations in antiferromagnetic $CaFe_2As_2$. *Phys. Rev. Lett.* **102,** 187206 (2009).
63. Zhao, J. *et al.* Spin waves and magnetic exchange interactions in $CaFe_2As_2$. *Nature Phys.* **5,** 555–560 (2009).
64. Lv, W., Wu, J. & Phillips, P. Orbital ordering induces structural phase transition and the resistivity anomaly in iron pnictides. *Phys. Rev. B* **80,** 224506 (2009).
65. Kou, S-P., Li, T. & Weng, Z-Y. Coexistence of itinerant electrons and local moments in iron-based superconductors. *Europhys. Lett.* **88,** 17010 (2009).
66. Johannes, M. D. & Mazin, I. I. Microscopic origin of magnetism and magnetic interactions in ferropnictides. *Phys. Rev. B* **79,** 220510(R) (2009).
67. de la Cruz, C. *et al.* Magnetic order close to superconductivity in the iron-based layered $LaO_{1-x}F_xFeAs$ systems. *Nature* **453,** 899–902 (2008).
68. Jesche, A., Krellner, C., de Souza, M., Lang, M. & Geibel, C. Coupling between the structural and magnetic transition in CeFeAsO. *Phys. Rev. B* **81,** 134525 (2010).
69. Chu, J-H., Analytis, J. G., Kucharczyk, C. & Fisher, I. R. Determination of the phase diagram of the electron-doped superconductor $Ba(Fe_{1-x}Co_x)_2As_2$. *Phys. Rev. B* **79,** 014506 (2009).
70. Chandra, P., Coleman, P. & Larkin, A. I. Ising transition in frustrated Heisenberg models. *Phys. Rev. Lett.* **64,** 88–91 (1989).
71. Urbano, R. R. *et al.* Distinct high-T transitions in underdoped $Ba_{1-x}K_xFe_2As_2$. Preprint at http://arxiv.org/abs/1005.3718 (2010).
72. de la Cruz, C. *et al.* Lattice distortion and magnetic quantum phase transition in $CeFeAs_{1-x}P_xO$. *Phys. Rev. Lett.* **104,** 017204 (2010).
73. Chen, T. Y., Tesanovic, Z., Liu, R. H., Chen, X. H. & Chien, C. L. A BCS-like gap in the superconductor $SmFeAsO_{0.85}F_{0.15}$. *Nature* **453,** 1224–1227 (2008).
74. Grafe, H-J. *et al.* ^{75}As NMR studies of superconducting $LaFeAsO_{0.9}F_{0.1}$. *Phys. Rev. Lett.* **101,** 047003 (2008).
75. Matano, K. *et al.* Spin-singlet superconductivity with multiple gaps in $PrFeAsO_{0.89}F_{0.11}$. *Europhys. Lett.* **83,** 57001 (2008).
76. Ning, F. *et al.* ^{59}Co and ^{75}As NMR investigation of electron-doped high T_c superconductor $BaFe_{1.8}Co_{0.2}As_2$ ($T_c = 22$ K). *J. Phys. Soc. Jpn* **77,** 103705 (2008).
77. Shimizu, Y. *et al.* Pressure-induced antiferromagnetic fluctuations in the pnictide superconductor $FeSe_{0.5}Te_{0.5}$: ^{125}Te NMR study. *J. Phys. Soc. Jpn* **78,** 123709. (2009).
78. Graser, S., Maier, T. A., Hirschfeld, P. J. & Scalapino, D. J. Near-degeneracy of several pairing channels in multiorbital models for the Fe pnictides. *New J. Phys.* **11,** 025016 (2009).
79. Hicks, C. W. *et al.* Limits on the superconducting order parameter in $NdFeAsO_{1-x}F_y$ from scanning SQUID microscopy. *J. Phys. Soc. Jpn* **78,** 013708 (2009).
80. Zhang, X. *et al.* Observation of the Josephson effect in $Pb/Ba_{1-x}K_xFe_2As_2$ single crystal junctions. *Phys. Rev. Lett.* **102,** 147002 (2009).
81. Wu, J. & Phillips, P. Experimental detection of sign-reversal pairing in iron-based superconductors. *Phys. Rev. B* **79,** 092502 (2009).

82. Parker, D. & Mazin, I. I. Possible phase-sensitive tests of pairing symmetry in pnictide superconductors. *Phys. Rev. Lett.* **102,** 227007 (2009).
83. Chen, W-Q., Ma, F., Lu, Z-Y. & Zhang, F-C. π junction to probe antiphase *s*-wave pairing in iron pnictide superconductors. *Phys. Rev. Lett.* **103,** 207001 (2009).
84. Chen, C-T., Tsuei, C. C., Ketchen, M. B., Ren, Z-A. & Zhao, Z. X. Integer and half-integer flux-quantum transitions in a niobium–iron pnictide loop. *Nature Phys.* **6,** 260–264 (2010).
85. Hanaguri, T., Niitaka, S., Kuroki, K. & Takagi, H. Unconventional *s*-wave superconductivity in Fe(Se, Te). *Science* **328,** 474–476 (2010).
86. Fernandes, R. M. *et al.* Unconventional pairing in the iron arsenide superconductors. *Phys. Rev. B* **81,** 140501 (2010).
87. Yu, G., Li, Y., Motoyama, E. M. & Greven, M. A universal relationship between magnetic resonance and superconducting gap in unconventional superconductors. *Nature Phys.* **5,** 873–875 (2009).
88. Shamoto, S. *et al.* Inelastic neutron scattering study on the resonance mode in an optimally doped superconductor $LaFeAsO_{0.92}F_{0.08}$. Preprint at http://arxiv.org/abs/1006.4640 (2010).
89. Christianson, A. D. *et al.* Unconventional superconductivity in $Ba_{0.6}K_{0.4}Fe_2As_2$ from inelastic neutron scattering. *Nature* **456,** 930–932 (2008).
90. Chi, S. *et al.* Inelastic neutron-scattering measurements of a three-dimensional spin resonance in the FeAs-based $BaFe_{1.9}Ni_{0.1}As_2$ superconductor. *Phys. Rev. Lett.* **102,** 107006 (2009).
91. Lumsden, M. D. *et al.* Two-dimensional resonant magnetic excitation in $BaFe_{1.84}Co_{0.16}As_2$. *Phys. Rev. Lett.* **102,** 107005 (2009).
92. Wang, M. *et al.* Electron-doping evolution of the low-energy spin excitations in the iron arsenide $BaFe_{2-x}Ni_xAs_2$ superconductors. *Phys. Rev. B* **81,** 174524 (2010).
93. Qiu, Y. *et al.* Spin gap and resonance at the nesting wave vector in superconducting $FeSe_{0.4}Te_{0.6}$. *Phys. Rev. Lett.* **103,** 067008 (2009).
94. Wen, J. *et al.* Effect of magnetic field on the spin resonance in $FeTe_{0.5}Se_{0.5}$ as seen via inelastic neutron scattering $FeSe_{0.4}Te_{0.6}$. *Phys. Rev. B* **81,** 100513 (2010).
95. Chubukov, A. V., Efremov, D. V. & Eremin, I. Magnetism, superconductivity, and pairing symmetry in iron-based superconductors. *Phys. Rev. B* **78,** 134512 (2008).
96. Maier, T. A., Graser, S., Scalapino, D. J. & Hirschfeld, P. J. Neutron scattering resonance and the iron-pnictide superconducting gap. *Phys. Rev. B* **79,** 134520 (2009).
97. Zhao, J. *et al.* Resonance as a probe of the electron superconducting gap in $BaFe_{1.9}Ni_{0.1}As_2$. *Phys. Rev. B* **81,** 180505(R) (2010).
98. Yashima, M. *et al.* Strong-coupling spin-singlet superconductivity with multiple full gaps in hole-doped $Ba_{0.6}K_{0.4}Fe_2As_2$ probed by ^{57}Fe-NMR. *J. Phys. Soc. Jpn* **78,** 103702 (2009).
99. Parker, D., Dolgov, O. V., Korshunov, M. M., Golubov, A. A. & Mazin, I. I. Extended $s_{\pm}$ scenario for the nuclear spin-lattice relaxation rate in superconducting pnictides. *Phys. Rev. B* **78,** 134524 (2008).
100. Mishra, V., Vorontsov, A., Hirschfeld, P. J. & Vekhter, I. Theory of thermal conductivity in extended-*s* state superconductors: Application to ferropnictides. *Phys. Rev. B* **80,** 224525 (2009).
101. Luo, X. G. *et al.* Quasiparticle heat transport in single-crystalline $Ba_{1-x}K_xFe_2As_2$: Evidence for a *k*-dependent superconducting gap without nodes. *Phys. Rev. B* **80,** 140503(R) (2009).
102. Tanatar, M. A. *et al.* Doping dependence of heat transport in the iron–arsenide superconductor $Ba(Fe_{1-x}Co_x)_2As_2$: From isotropic to a strongly *k*-dependent gap structure. *Phys. Rev. Lett.* **104,** 067002 (2010).
103. Dong, J. K. *et al.* Thermal conductivity of overdoped $BaFe_{1.73}Co_{0.27}As_2$ single crystal: Evidence for nodeless multiple superconducting gaps and interband interactions. *Phys. Rev. B* **81,** 094520 (2010).
104. Ding, L. *et al.* Nodeless superconducting gap in electron-doped $BaFe_{1.9}Ni_{0.1}As_2$ probed by quasiparticle heat transport. *New J. Phys.* **11,** 093018 (2009).
105. Dong, J. K. *et al.* Quantum criticality and nodal superconductivity in the FeAs-based superconductor KFe_2As_2. *Phys. Rev. Lett.* **104,** 087005 (2010).
106. Hashimoto, K. *et al.* Line nodes in the energy gap of high-temperature superconducting $BaFe_2(As_{1-x}P_x)_2$ from penetration depth and thermal conductivity measurements. *Phys. Rev. B* **81,** 220501(R) (2010).
107. Mishra, V. *et al.* Lifting of nodes by disorder in extended-*s*-state superconductors: Application to ferropnictides. *Phys. Rev. B* **79,** 094512 (2009).
108. Reid, J-Ph. *et al.* Nodes in the gap structure of the iron–arsenide superconductor $Ba(Fe_{1-x}Co_x)_2As_2$ from *c*-axis heat transport measurements. *Phys. Rev. B* **82,** 064501 (2010).
109. Laad, M. S. & Craco, L. Theory of multiband superconductivity in iron pnictides. *Phys. Rev. Lett.* **103,** 017002 (2009).
110. Zeng, B. *et al.* Anisotropic structure of the order parameter in $FeSe_{0.4}Te_{0.6}$ revealed by angle resolved specific heat. Preprint at http://arxiv.org/abs/1007.3597 (2010).
111. Hashimoto, K. *et al.* Microwave surface-impedance measurements of the magnetic penetration depth in single crystal $Ba_{1-x}K_xFe_2As_2$ superconductors: Evidence for a disorder-dependent superfluid density. *Phys. Rev. Lett.* **102,** 207001 (2009).
112. Kim, H. *et al.* London penetration depth in $Ba(Fe_{1-x}T_x)_2As_2$ (T = Co, Ni) superconductors irradiated with heavy ions. Preprint at http://arxiv.org/abs/1003.2959 (2010).
113. Martin, C. *et al.* Nonexponential London penetration depth of FeAs-based superconducting $RFeAsO_{0.9}F_{0.1}$ (R = La, Nd) single crystals. *Phys. Rev. Lett.* **102,** 247002 (2009).
114. Luan, L. *et al.* Local measurement of the penetration depth in the pnictide superconductor $Ba(Fe_{0.95}Co_{0.05})_2As_2$. *Phys. Rev. B* **81,** 100501 (2010).
115. Gofryk, K. *et al.* Doping-dependent specific heat study of the superconducting gap in $Ba(Fe_{1-x}Co_x)_2As_2$. *Phys. Rev. B* **81,** 184518 (2010).
116. Kim, J. S. *et al.* Specific heat vs field in the 30 K superconductor $BaFe_2(As_{0.7}P_{0.3})_2$. *Phys. Rev. B* **81,** 214507 (2010).
117. Hardy, F. *et al.* Doping evolution of superconducting gaps and electronic densities of states in $Ba(Fe_{1-x}Co_x)_2As_2$ iron pnictides. Preprint at http://arxiv.org/abs/1007.2218 (2010).
118. Popovich, P. *et al.* Specific heat of $Ba_{0.68}K_{0.32}Fe_2As_2$: Evidence for multiband strong-coupling superconductivity. *Phys. Rev. Lett.* **105,** 027003 (2010).
119. Mu, G. *et al.* Low temperature specific heat of the hole-doped $Ba_{0.6}K_{0.4}Fe_2As_2$ single crystals. *Phys. Rev. B* **79,** 174501 (2009).
120. Welp, U. *et al.* Specific heat and phase diagrams of single crystal iron pnictide superconductors. *Physica C* **469,** 575–581 (2009).
121. Bang, Y. Volovik effect in the ±*s*-wave state for the iron-based superconductors. *Phys. Rev. Lett.* **104,** 217001 (2010).
122. Bud'ko, S. L., Ni, N. & Canfield, P. C. Jump in specific heat at the superconducting transition temperature in $Ba(Fe_{1-x}Co_x)_2As_2$ and $Ba(Fe_{1-x}Ni_x)_2As_2$ single crystals. *Phys. Rev. B* **79,** 220516 (2009).
123. Kant, C. *et al.* Magnetic and superconducting transitions in $Ba_{1-x}K_xFe_2As_2$ studied by specific heat. *Phys. Rev. B* **81,** 014529 (2010).
124. Hardy, F. *et al.* Calorimetric evidence of multiband superconductivity in $Ba(Fe_{0.925}Co_{0.075})_2As_2$ single crystals. *Phys. Rev. B* **81,** 060501(R) (2010).
125. Ni, N. *et al.* Phase diagrams of $Ba(Fe_{1-x}M_x)_2As_2$ single crystals (M = Rh and Pd). *Phys. Rev. B* **80,** 024511 (2009).
126. Hu, R., Bozin, E. S., Warren, J. B. & Petrovic, C. Superconductivity, magnetism, and stoichiometry of single crystals of $Fe_{1+y}(Te_{1-x}S_x)_z$. *Phys. Rev. B* **80,** 214514 (2009).
127. Analytis, J. G. *et al.* Bulk superconductivity and disorder in single crystals of LaFePO. Preprint at http://arxiv.org/abs/0810.5368 (2008).
128. Baumbach, R. E. *et al.* Superconductivity in LnFePO (Ln = La, Pr and Nd) single crystals. *New J. Phys.* **11,** 025018 (2009).
129. Braithwaite, D., Lapertot, G., Knafo, W. & Sheikin, I. Evidence for anisotropic vortex dynamics and Pauli limitation in the upper critical field of $FeSe_{1-x}Te_x$. *J. Phys. Soc. Jpn* **79,** 053703 (2010).
130. Sato, M. *et al.* Studies on effects of impurity doping and NMR measurements of La 1111 and/or Nd 1111 Fe-pnictide superconductors. *J. Phys. Soc. Jpn* **79,** 014710 (2010).
131. Zaanen, J. Specific-heat jump at the superconducting transition and the quantum critical nature of the normal state of pnictide superconductors. *Phys. Rev. B* **80,** 212502 (2009).
132. Kogan, V. G. Pair breaking in iron pnictides. *Phys. Rev. B* **80,** 214532 (2009).
133. Tarantini, C. *et al.* Suppression of the critical temperature of superconducting NdFeAs(OF) single crystals by Kondo-like defect sites induced by α-particle irradiation. *Phys. Rev. Lett.* **104,** 087002 (2010).
134. Muschler, B. *et al.* Band- and momentum-dependent electron dynamics in superconducting $Ba(Fe_{1-x}Co_x)_2As_2$ as seen via electronic Raman scattering. *Phys. Rev. B* **80,** 180510 (2009).
135. Williams, T. J. *et al.* Muon spin rotation measurement of the magnetic field penetration depth in $Ba(Fe_{0.926}Co_{0.074})_2As_2$: Evidence for multiple superconducting gaps. *Phys. Rev. B* **80,** 094501 (2009).
136. Yin, Y. *et al.* Scanning tunneling spectroscopy and vortex imaging in the iron pnictide superconductor $BaFe_{1.8}Co_{0.2}As_2$. *Phys. Rev. Lett.* **102,** 097002 (2009).
137. Boeri, L., Calandra, M., Mazin, I. I., Dolgov, O.V. & Mauri, F. Effects of magnetism and doping on the electron–phonon coupling in $BaFe_2As_2$. *Phys. Rev. B* **82,** 020506(R) (2010).
138. Liu, R. H. *et al.* A large iron isotope effect in $SmFeAsO_{1-x}F_x$ and $Ba_{1-x}K_xFe_2As_2$. *Nature* **459,** 64–67 (2009).
139. Shirage, P. M. *et al.* Absence of an appreciable iron isotope effect on the transition temperature of the optimally doped $SmFeAsO_{1-y}$ superconductor. *Phys. Rev. Lett.* **105,** 037004 (2010).
140. Qazilbash, M. M. *et al.* Electronic correlations in the iron pnictides. *Nature Phys.* **5,** 647–650 (2009).
141. Yang, W. L. *et al.* Evidence for weak electronic correlations in iron pnictides. *Phys. Rev. B* **80,** 014508 (2009).
142. Yin, Z. P., Haule, K. & Kotliar, G. Magnetism and charge dynamics in iron pnictides. Preprint at http://arxiv.org/abs/1007.2867 (2010).
143. Wang, X. F. *et al.* Anisotropy in the electrical resistivity and susceptibility of superconducting $BaFe_2As_2$ single crystals. *Phys. Rev. Lett.* **102,** 117005 (2009).

144. Bonville, P., Rullier-Albenque, F., Colson, D. & Forget, A. Incommensurate spin density wave in Co-doped $BaFe_2As_2$. *Europhys. Lett.* **89,** 67008 (2010).
145. Diallo, S. O. *et al.* Paramagnetic spin correlations in $CaFe_2As_2$ single crystals. *Phys. Rev. B* **81,** 214407 (2010).
146. Ning, F. L. *et al.* Contrasting spin dynamics between underdoped and overdoped $Ba(Fe_{1-x}Co_x)_2As_2$. *Phys. Rev. Lett.* **104,** 037001 (2010).
147. Dai, J., Si, Q., Zhu, J-X. & Abrahams, E. Iron pnictides as a new setting for quantum criticality. *Proc. Natl Acad. Sci.* **106,** 4118–4121 (2010).
148. Nakai, Y. *et al.* Unconventional superconductivity and antiferromagnetic quantum critical behaviour in the isovalent-doped $BaFe_2(As_{1-x}P_x)_2$. Preprint at http://arxiv.org/abs/1005.2853 (2010).
149. Goko, T. *et al.* Superconducting state coexisting with a phase-separated static magnetic order in $(Ba,K)Fe_2As_2$, $(Sr,Na)Fe_2As_2$, and $CaFe_2As_2$. *Phys. Rev. B* **80,** 024508 (2009).
150. Laplace, Y., Bobroff, J., Rullier-Albenque, F., Colson, D. & Forget, A. Atomic coexistence of superconductivity and incommensurate magnetic order in the pnictide $Ba(Fe_{1-x}Co_x)_2As_2$. *Phys. Rev. B* **80,** 140501 (2009).

Acknowledgements

The authors would like to thank P. J. Hirschfeld, J. W. Lynn, I. I. Mazin, D. J. Scalapino and L. Taillefer for discussions and comments. This research was supported by AFOSR-MURI under FA9550-09-1-0603.

Additional information

The authors declare no competing financial interests. Reprints and permissions information is available online at http://npg.nature.com/reprintsandpermissions. Correspondence and requests for materials should be addressed to J.P.